Quantum statistical properties of nondegenerate optical parametric symmetric coupler

1999 J. Phys. A: Math. Gen. 32 3457

(http://iopscience.iop.org/0305-4470/32/19/301)

J. Phys. A: Math. Gen. **32** (1999) 3457–3483. Printed in the UK PII: S0305-4470(99)00108-0

Quantum statistical properties of nondegenerate optical parametric symmetric coupler

M Sebawe Abdalla†, Faisal A A El-Orany‡§ and J Peřina‡

† Mathematics Department, College of Science, King Saud University, PO Box 2455, Riyadh 11451, Saudi Arabia

‡ Department of Optics and Joint Laboratory of Optics, Palacký University, 17 Listopadu 50, 772 07 Olomouc, Czech Republic

Received 9 December 1998, in final form 9 February 1999

Abstract. In the framework of Hamiltonian formalism the quantum statistical properties of an optical field propagating inside a directional coupler operating by nondegenerate parametric amplification are studied. We investigate the effect of switching between the input modes and the outgoing fields from the coupler. Particular attention is paid to two-mode squeezing, the second-order correlation function, quasiprobability distribution functions, and photon-number distribution. Incident number and coherent states are considered. It has been shown that when one of the modes enters the coupler in the Fock state $|1\rangle$ and the other modes are in vacuum states, the coupler can serve as a generator of a coherent state. Furthermore, regimes for the generation and transmission of squeezed and/or sub-Poissonian light are found.

1. Introduction

Recently a resurgence of interest has focused on the problem of optical control of switching, modulating and frequency selecting in guided wave schemes. Such schemes are important in both optical communication networks and in generating new fields of nonclassical light. The most important optical devices representing these schemes are nonlinear couplers which consist of two or more waveguides connected mutually by means of evanescent waves. In one or more of these waveguides a nonlinear process takes place. When a flux is introduced into only one of the waveguides, an output from either waveguide occurs, which can be controlled by the device design and the input flux. The action of nonlinear couplers has been demonstrated experimentally in planar structures [1, 2], dual optical fibres [3], and also for certain organic polymers [4].

Since the pioneering work on nonlinear couplers of Jensen and Maier [5], a series of papers have been devoted to the study of this important optical device. Particular attention has been paid to quantum statistical properties [6–10] in relation to quantum noise and the generation and transmission of nonclassical light. In fact, the original model proposed by Jensen and Maier was recognized to have potential applicability in optical communications as an intensity-dependent routing switch [11] and its stability analysis [12] was performed. Such generation and transmission of nonclassical light can be very effective as a consequence of the evanescent waves involved in the interaction. We mention that field-dependent effects require

§ On leave from: Department of Mathematics and Computer Science, Faculty of Science, Suez Canal University, Ismailla, Egypt.

0305-4470/99/193457+27$19.50

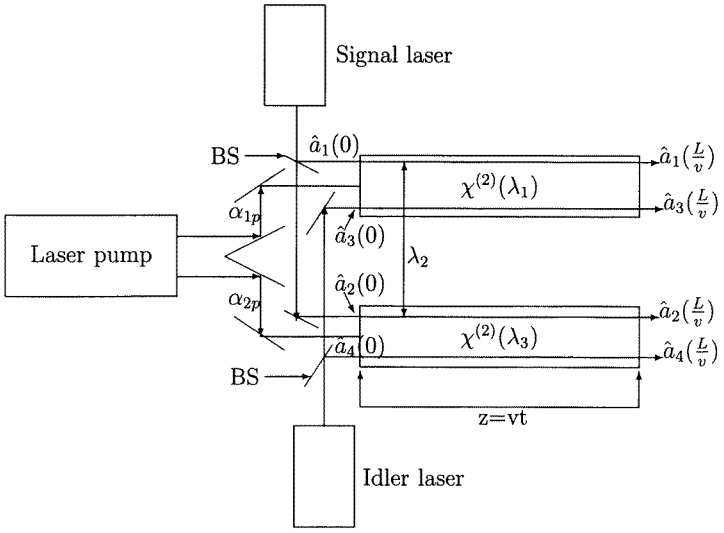

Figure 1. Scheme of realization of interaction in (1.1); BS are beam splitters.

further investigation of their dependence on phase mismatch in the medium [13]. Furthermore, interesting quantum statistical properties of nonlinear co-/contra-directional couplers were derived, composed of two nonlinear waveguides operating by second-harmonic generation [9, 14], the nondegenerate optical parametric process of frequency down-conversion [15], optical Kerr-like effects [16–21] and Raman scattering ([22], and references therein). It is worthwhile to mention that the revivals and collapses of the oscillations in mean photon number occurring for the well known Jaynes–Cummings model [23] has been also observed in the codirectional nonlinear couplers composed of Kerr-nonlinear waveguides [18, 19].

In this paper we concentrate on studying the statistical properties of an optical field propagating within a directional coupler containing a parametric amplifying medium. Our starting point is the Hamiltonian, which represents a nonlinear directional coupler composed of two nonlinear waveguides (taking into account the case of a strong pump, where non-depleting intensity is included in the amplifier coupling constant). This model can be described by

$$\frac{H}{\hbar} = \lambda_1(\hat{a}_1\hat{a}_3 + \hat{a}_1^\dagger\hat{a}_3^\dagger) + \lambda_2(\hat{a}_1\hat{a}_2^\dagger + \hat{a}_1^\dagger\hat{a}_2) + \lambda_3(\hat{a}_2\hat{a}_4 + \hat{a}_2^\dagger\hat{a}_4^\dagger) \tag{1.1}$$

and the corresponding scheme is illustrated in figure 1. Two waveguides of length L operating by nondegenerate optical parametric processes with signal beams described by annihilation operators $\hat{a}_1$ and $\hat{a}_2$ and idler beams described by $\hat{a}_3$ and $\hat{a}_4$ are pumped by strong laser beams of complex amplitudes α_{1p} and α_{2p}, respectively, and signals are coupled linearly by evanescent waves with the strength λ_2; v is the speed of the waves (dispersion is neglected) and $\chi^{(2)}$ is quadratic susceptibility. The coupling constants λ_1 and λ_3 include the pumping amplitudes. Instead of initial coherent states at the signal and idler beams, the Fock states generated, for instance, in micromaser can be introduced. Outgoing fields are detected as single or compound modes by means of homodyne, photocounting or coincidince detection. As we assume one-passage propagation, losses in the beams can be neglected. In other cases they can be described in the standard quantum way in the form of interaction of light beams with reservoirs, as, for instance, described in [24]. However, one generally finds that nonclassical properties of light beams degrade due to the effect of the reservoir: less by the damping (which may be by several orders weaker than the nonlinear coupling), more due to by the influence of the non-zero mean

number of reservoir oscillators.

Further, the values of the coupling constants $\lambda_1, \lambda_2, \lambda_3$ are chosen for simplicity of calculation and illustration of the physical behaviour of the system. We mainly demonstrate the effect of their mutual relations and their magnitudes are not important for such demonstration. For an experimental realization these values can be estimated as $(10^{11}$–$10^{12})$ s^{-1}, provided that the pumping laser of power in mW is used, producing about 10^{19} photons s^{-1}, which is sufficient power to allow us to neglect quantum noise in the pumping beams. Then all the effects shown are interpreted on a correspondingly reduced timescale. Initial state amplitudes or photon numbers are chosen in units because switching properties are examined on the quantum level of single photons.

Clearly, the Hamiltonian has a kind of symmetry which will be helpful to reduce the number of equations. For example, if one takes $\hat{a}_1 \longleftrightarrow \hat{a}_2$, $\hat{a}_3 \longleftrightarrow \hat{a}_4$ and $\lambda_1 \longleftrightarrow \lambda_3$, the Hamiltonian (1.1) is still invariant.

The above Hamiltonian was considered by Janszky *et al* [15] (taking into consideration that the coupling parameters λ_1 and λ_2 are equal), where they discussed the propagation of a quantum field in a coupler when the channels contain a parametric amplifying medium. This situation occurs if one or both channels [25] are made from a second-order nonlinear material realizing a parametric process (down conversion). They have found two operation regimes: one under threshold, where the amplification is less effective than the coupling between channels, and another above threshold, where the amplification constant is greater than the coupling constant. However, the above Hamiltonian (1.1) has the advantage of showing spatial effects (e.g. switching between the channels), where the coupling parameters will play a great role in controlling this phenomena. This is demonstrated in the following. Also, we give more details for the quantum statistical properties of this model compared with [15]. We study these properties taking into account the coupling between idler modes due to the evanescent field between the waveguides [26]. Moreover, we wish to treat problems of propagation in the Hamiltonian formalism, assuming that the energy of the system does not have directionality. However, in the case where all waves are propagating with the same velocity, time and space relate by the velocity of propagation v, $z = vt$. Our study of the model is organized as follows: in section 2 we describe the model under discussion together with the solution of the equations of motion, in section 3 we derive two-mode squeezing characteristics of generated light, section 4 is devoted to a discussion of photon antibunching, section 5 includes results for quasidistribution functions, section 6 includes a discussion of photon-number distribution for the output modes, and finally we summarize our main conclusions in section 7.

2. Equations of motion and their solutions

The Heisenberg equation of motion for any operator $\hat{O}$ is given by

$$\frac{\mathrm{d}\hat{O}}{\mathrm{d}t} = \frac{\partial \hat{O}}{\partial t} + \frac{1}{\mathrm{i}\hbar}[\hat{O}, H] \tag{2.1}$$

where $[\ldots,\ldots]$ represents the commutator.

Therefore we can describe the propagation of the field operators by the following equations:

$$\frac{\mathrm{d}\hat{a}_1}{\mathrm{d}t} = -\mathrm{i}\lambda_1\hat{a}_3^\dagger - \mathrm{i}\lambda_2\hat{a}_2 \tag{2.2a}$$

$$\frac{\mathrm{d}\hat{a}_2}{\mathrm{d}t} = -\mathrm{i}\lambda_2\hat{a}_1 - \mathrm{i}\lambda_3\hat{a}_4^\dagger \tag{2.2b}$$

$$\frac{\mathrm{d}\hat{a}_3}{\mathrm{d}t} = -\mathrm{i}\lambda_1\hat{a}_1^\dagger \tag{2.2c}$$

$$\frac{\mathrm{d}\hat{a}_4}{\mathrm{d}t} = -\mathrm{i}\lambda_3\hat{a}_2^\dagger \tag{2.2d}$$

having the conservation law

$$\frac{\mathrm{d}}{\mathrm{d}t}[\hat{a}_1^\dagger\hat{a}_1 + \hat{a}_2^\dagger\hat{a}_2 - \hat{a}_3^\dagger\hat{a}_3 - \hat{a}_4^\dagger\hat{a}_4] = 0.$$

The exact solution of the above equations has the following form:

$$\hat{a}_1(t) = f_1(t)\hat{a}_1(0) + \mathrm{i}f_2(t)\hat{a}_2(0) - \mathrm{i}f_3(t)\hat{a}_3^\dagger(0) + f_4(t)\hat{a}_4^\dagger(0) \tag{2.3a}$$

$$\hat{a}_2(t) = g_2(t)\hat{a}_2(0) + \mathrm{i}g_1(t)\hat{a}_1(0) + g_3(t)\hat{a}_3^\dagger(0) - \mathrm{i}g_4(t)\hat{a}_4^\dagger(0) \tag{2.3b}$$

$$\hat{a}_3(t) = h_3(t)\hat{a}_3(0) + h_2(t)\hat{a}_2^\dagger(0) - \mathrm{i}h_1(t)\hat{a}_1^\dagger(0) - \mathrm{i}h_4(t)\hat{a}_4(0) \tag{2.3c}$$

$$\hat{a}_4(t) = l_4(t)\hat{a}_4(0) + l_1(t)\hat{a}_1^\dagger(0) - \mathrm{i}l_2(t)\hat{a}_2^\dagger(0) - \mathrm{i}l_3(t)\hat{a}_3(0) \tag{2.3d}$$

where $\hat{a}_j(0)$ are the input operators and the time-dependent functions are given by

$$f_1(t) = \cos(t\Omega_1)\cosh^2\phi - \cosh(t\Omega_2)\sinh^2\phi \tag{2.4a}$$

$$f_2(t) = \frac{\lambda_3}{2}\left[\frac{\sin(t\Omega_1)}{\Omega_1} - \frac{\sinh(t\Omega_2)}{\Omega_2}\right]\sinh(2\phi) - \lambda_2\left[\frac{\sinh(t\Omega_1)}{\Omega_1}\cosh^2\phi - \frac{\sinh(t\Omega_2)}{\Omega_2}\sinh^2\phi\right] \tag{2.4b}$$

$$f_3(t) = \lambda_1\left[\frac{\sin(t\Omega_1)}{\Omega_1}\cosh^2\phi - \frac{\sinh(t\Omega_2)}{\Omega_2}\sinh^2\phi\right] \tag{2.4c}$$

$$f_4(t) = \tfrac{1}{2}[\cos(t\Omega_1) - \cosh(t\Omega_2)]\sinh(2\phi) \tag{2.4d}$$

$$h_1(t) = \frac{\lambda_2}{2}\left[\frac{\sin(t\Omega_3)}{\Omega_3} - \frac{\sinh(t\Omega_4)}{\Omega_4}\right]\sinh(2\theta) + \lambda_1\left[\frac{\sinh(t\Omega_4)}{\Omega_4}\cosh^2\theta - \frac{\sin(t\Omega_3)}{\Omega_3}\sinh^2\theta\right] \tag{2.5a}$$

$$h_2(t) = \tfrac{1}{2}[\cosh(t\Omega_4) - \cos(t\Omega_3)]\sinh(2\theta) \tag{2.5b}$$

$$h_3(t) = \cosh(t\Omega_4)\cosh^2\theta - \cos(t\Omega_3)\sinh^2\theta \tag{2.5c}$$

$$h_4(t) = \frac{\lambda_3}{2}\left[\frac{\sin(t\Omega_3)}{\Omega_3} - \frac{\sinh(t\Omega_4)}{\Omega_4}\right]\sinh(2\theta) \tag{2.5d}$$

where

$$\Omega_1 = [k_1^2\cosh^2\phi + \lambda_3^2\sinh^2\phi - \lambda_2\lambda_3\sinh(2\phi)]^{\frac{1}{2}} \tag{2.6a}$$

$$\Omega_2 = [k_1^2\sinh^2\phi + \lambda_3^2\cosh^2\phi - \lambda_2\lambda_3\sinh(2\phi)]^{\frac{1}{2}} \tag{2.6b}$$

and

$$\phi = \frac{1}{2}\tanh^{-1}\left(\frac{2\lambda_2\lambda_3}{\lambda_2^2 + \lambda_3^2 - \lambda_1^2}\right) \tag{2.7}$$

with $k_1 = \sqrt{\lambda_2^2 - \lambda_1^2}$. Other coefficients can be obtained with the help of the substitution $\lambda_1 \longleftrightarrow \lambda_3$ and hence

$$\begin{aligned} &\Omega_1 \longleftrightarrow \Omega_3 \qquad \Omega_2 \longleftrightarrow \Omega_4 \qquad \phi \longleftrightarrow \theta \\ &(f_1(t), f_2(t), f_3(t), f_4(t)) \longleftrightarrow (g_2(t), g_1(t), g_4(t), g_3(t)) \\ &(h_1(t), h_2(t), h_3(t), h_4(t)) \longleftrightarrow (l_2(t), l_1(t), l_4(t), l_3(t)). \end{aligned} \tag{2.8}$$

In the forthcoming discussion we restrict ourselves on the relations for modes 1 and 3, keeping in mind that the other relations for modes 2 and 4 can be obtained from (2.8) using the following substitutions: $\hat{a}_1 \longleftrightarrow \hat{a}_2$, $\hat{a}_3 \longleftrightarrow \hat{a}_4$ and $\lambda_1 \longleftrightarrow \lambda_3$.

From equations (2.3) it is easy to check that the well known commutation relations between Boson operators are satisfied, which leads to the following relations:

$$\begin{aligned} &f_1^2(t) + f_2^2(t) - f_3^2(t) - f_4^2(t) = 1 \\ &h_3^2(t) + h_4^2(t) - h_1^2(t) - h_2^2(t) = 1 \\ &f_1(t)h_1(t) = f_2(t)h_2(t) + f_3(t)h_3(t) + f_4(t)h_4(t). \end{aligned} \tag{2.9}$$

Here we point out that the existence of the negative sign in the denominator of equation (2.7) can restrict our choice of the coupling parameters λ_j.

In subsequent sections we use the results obtained here to discuss the statistical properties of the Hamiltonian model (1.1), where we consider the squeezing and antibunching phenomena. We shall also examine the behaviour of quasiprobability distribution functions and the photon-number distribution.

3. Two-mode squeezing phenomenon

One of the important nonclassical phenomena in the framework of quantum theory, owing to its application in optical communications and high precision measurements, is quadrature squeezing of vacuum fluctuations. Such a phenomenon is characterized by the property that the variance of the quadrature operator is less than the value associated with the vacuum noise level. This phenomenon can be seen in simple models of a number of nonlinear optical processes such as harmonic generation [27, 28], four-wave mixing processes [29, 30] and Raman and hyper-Raman processes [24, 31, 32].

The definition of single-mode squeezing has been extended to two-mode interaction [33, 34]. The parametric amplifier in a cavity is a particularly important example since it can ideally produce squeezed light with characteristics akin to single- and two-mode when operating in degenerate and nondegenerate regimes, respectively [35].

Here we study two-mode squeezing using quadrature operators $\hat{X}$ and $\hat{Y}$ which are defined as

$$\hat{X} = \tfrac{1}{2}[\hat{a}_k + \hat{a}_k^\dagger + \hat{a}_j + \hat{a}_j^\dagger] \tag{3.1a}$$

$$\hat{Y} = \frac{1}{2i}[\hat{a}_k - \hat{a}_k^\dagger + \hat{a}_j - \hat{a}_j^\dagger] \tag{3.1b}$$

where $k \neq j$; $k, j = 1, 2, 3, 4$. These quadratures satisfy the commutation relation

$$[\hat{X}, \hat{Y}] = i \tag{3.1c}$$

and then the uncertainty relation holds

$$\langle(\triangle\hat{X})^2\rangle\langle(\triangle\hat{Y})^2\rangle \succeq \tfrac{1}{4}. \tag{3.1d}$$

Therefore, two-mode squeezing occurs when

$$2\langle(\triangle\hat{X})^2\rangle - 1 < 0 \qquad \text{or} \qquad 2\langle(\triangle\hat{Y})^2\rangle - 1 < 0 \tag{3.1e}$$

where $\langle(\triangle\hat{X})^2\rangle = \langle\hat{X}^2\rangle - \langle\hat{X}\rangle^2$ is the variance of the quadrature operator $\hat{X}$ and zero has been taken as a measure of squeezing, i.e. squeezing occurs in the quadrature $\hat{X}$ (say) only when $2\langle(\triangle\hat{X})^2\rangle - 1$ is less than zero.

Since the electromagnetic field is guided inside the structure, exchange of energy between the two waveguides is possible because of the evanescent field between the waveguides [26]. So we can examine several cases of two-mode squeezing for this model using the input initial coherent states $\prod_{j=1}^{4} |\alpha\rangle_j$. The basic equations for this study are (2.3) and (3.1).

In the first case, two-mode squeezing for mode 1 and mode 4, i.e. for the signal mode in the first waveguide and the idler mode in the second waveguide, is described by

$$2\langle(\triangle\hat{X}_1)^2\rangle\exp(2\phi) = [\cosh\phi\cos(t\Omega_1) + \sinh\phi\cosh(t\Omega_2)]^2 + \left[(\lambda_3\cosh\phi - \lambda_2\sinh\phi)\frac{\sinh(t\Omega_2)}{\Omega_2} + (\lambda_3\sinh\phi - \lambda_2\cosh\phi)\frac{\sin(t\Omega_1)}{\Omega_1}\right]^2 \tag{3.2a}$$

$$2\langle(\triangle\hat{Y}_1)^2\rangle\exp(-2\phi) = [\cosh\phi\cos(t\Omega_1) - \sinh\phi\cosh(t\Omega_2)]^2 + \left[(\lambda_3\cosh\phi - \lambda_2\sinh\phi)\frac{\sinh(t\Omega_2)}{\Omega_2} - (\lambda_3\sinh\phi - \lambda_2\cosh\phi)\frac{\sin(t\Omega_1)}{\Omega_1}\right]^2. \tag{3.2b}$$

In the second case, two-mode squeezing for mode 1 and mode 2, i.e. for the signal modes in the first and second waveguides, is described by

$$\langle(\triangle\hat{X}_2)^2\rangle = \langle(\triangle\hat{Y}_2)^2\rangle = \tfrac{1}{2}[1 + f_3^2(t) + f_4^2(t) + g_2^2(t) + g_4^2(t)]. \tag{3.3}$$

In the third case, two-mode squeezing for mode 3 and mode 4, i.e. for the idler modes in the two waveguides, is described by

$$\langle(\triangle\hat{X}_4)^2\rangle = \langle(\triangle\hat{Y}_4)^2\rangle = \tfrac{1}{2}[1 + h_2^2(t) + h_3^2(t) + l_1^2(t) + l_2^2(t)]. \tag{3.4}$$

We can see from (3.2)–(3.4) that this coupler can generate squeezing, in terms of two-mode definition, only when considering the signal mode in the first waveguide and the idler mode in the second waveguide or the idler mode in the first waveguide and the signal mode in the second waveguide. So we concentrate on this case. In figure 2, we have plotted the squeezing component for the first case for different values of λ_j against time t. Curves A1 and A2 relate to the X_1-component corresponding to the two groups of values for λ_j, respectively, and, similarly, curves B1 and B2 relate to the Y_1-component. For λ_1 small, $\lambda_2 > \lambda_3 > \lambda_1$, i.e. when linear exchange between the waveguides is stronger than the nondegenerate parametric amplification inside the waveguides, we observe that squeezing is dominant in the first quadrature, having oscillatory behaviour; nevertheless the value of squeezing is negligible in the second component, see curves A1 and B1. Increasing the values of both λ_1 and λ_2 and keeping λ_3 as before, we observed squeezing in both the quadratures and its values were more pronounced than in the earlier case, with the maximum value of squeezing being in the first quadrature, see curves A2 and B2.

Thus, we can conclude that this system is able to generate squeezed light in terms of two-mode squeezing only when the signal and idler modes are considered in different waveguides and provided that the signal modes are coupled. The values of squeezing are well controllable by the values of coupling constants.

4. Second-order correlation function

Antibunched and/or sub-Poissonian light is an example of nonclassical light and can be determined from a photocounting-correlation measurement. In practice, the measurement can be performed in an experiment of the Hanbury Brown–Twiss type. As a measure for super-Poissonion (classical) and sub-Poissonion (nonclassical) phenomena of photons in the system, the normalized normal second-order correlation function can serve [36]:

$$g_j^{(2)}(t) = \frac{\langle\hat{a}_j^{\dagger 2}(t)\hat{a}_j^2(t)\rangle}{\langle\hat{a}_j^{\dagger}(t)\hat{a}_j(t)\rangle^2} = 1 + \frac{\langle(\triangle\hat{n}_j(t))^2\rangle - \langle\hat{a}_j^{\dagger}(t)\hat{a}_j(t)\rangle}{\langle\hat{a}_j^{\dagger}(t)\hat{a}_j(t)\rangle^2} \tag{4.1}$$

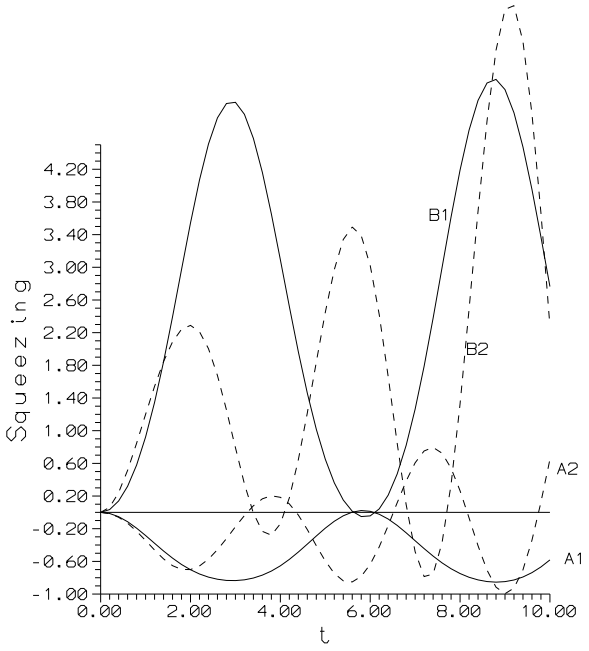

Figure 2. Two-mode squeezing phenomenon for the first case, for solid curves $\lambda_1 = 0.1$, $\lambda_2 = 1.25$ and $\lambda_3 = 0.5$; for dashed curves $\lambda_1 = 0.6$, $\lambda_2 = 2$ and $\lambda_3 = 0.5$.

where the subscript j relates to the jth mode and $\langle(\triangle\hat{n}_j(t))^2\rangle$ are the photon-number variances with $\hat{n}_j(t) = \hat{a}_j^\dagger(t)\hat{a}_j(t)$. Then it holds that $g_j^{(2)}(t) < 1$ for a sub-Poissonian distribution, $g_j^{(2)}(t) > 1$ for a super-Poissonian distribution and when $g_j^{(2)}(t) = 1$ a Poisson distribution of photons occurs. As is well known, the best examples for sub-Poissonian, super-Poissonian and Poissonian statistics are Fock state, chaotic field and coherent state, respectively.

On the other hand, it has been shown explicitly in [37, 38] that sub-Poissonian photon statistics need not be associated with antibunching, but can be accompanied by bunching. However, within the framework of the classical theory, light cannot be antibunched, i.e. antibunched light is a manifestation of a quantum effect. The basic formula to study this phenomenon is the two-time normalized intensity correlation function [38, 39]. For the jth mode, this function is defined by

$$g_j^{(2)}(t, t+\tau) = \frac{\langle\hat{a}_j^\dagger(t)\hat{a}_j^\dagger(t+\tau)\hat{a}_j(t+\tau)\hat{a}_j(t)\rangle}{\langle\hat{a}_j^\dagger(t)\hat{a}_j(t)\rangle\langle\hat{a}_j^\dagger(t+\tau)\hat{a}_j(t+\tau)\rangle}. \tag{4.2}$$

The importance of this function in the analysis of photon antibunching comes from the direct relation between this function and the joint detection probability of two photons, one at time t and another at time $t+\tau$. It is clear that using (4.2) for $\tau \to 0$ as a definition of bunching properties, then the bunching/antibunching and super-/sub-Poissonian statistics are in one-to-one correspondence. A more general definition of photon antibunching can be adopted [38,39] if $g_j^{(2)}(t, t+\tau)$ increases from its initial value at $\tau = 0$. This can be represented in equivalent differential form, assuming that $g_j^{(2)}(t, t+\tau)$ is a well behaved function in τ, as

$$K_j(t) = \frac{\partial g_j^{(2)}(t, t+\tau)}{\partial\tau}|_{\tau=0} > 0. \tag{4.3}$$

Photon bunching is given by the opposite condition ($K_j(t) < 0$); otherwise the photons are unbunched.

Here we turn our attention to trace the nonclassical effects for the model under discussion using the normalized second-order correlation function for the various modes when the initial input light modes are in number states $\prod_{j=1}^{4} |n\rangle_j$ as well as in the coherent states. Then, we extend our discussion to demonstrate the photon antibunching phenomenon for our model.

When the input light is in the number states, we have

$$\langle \hat{n}_1(t+\tau)\rangle_n = f_1^2(t+\tau)\bar{n}_1 + f_2^2(t+\tau)\bar{n}_2 + f_3^2(t+\tau)(\bar{n}_3+1) + f_4^2(t+\tau)(\bar{n}_4+1) \tag{4.4a}$$

$$\langle \hat{n}_3(t+\tau)\rangle_n = h_3^2(t+\tau)\bar{n}_3 + h_4^2(t+\tau)\bar{n}_4 + h_2^2(t+\tau)(\bar{n}_2+1) + h_1^2(t+\tau)(\bar{n}_1+1) \tag{4.4b}$$

and

$$\begin{aligned}\langle \hat{a}_1^\dagger(t)\hat{a}_1^\dagger(t+\tau)\hat{a}_1(t+\tau)\hat{a}_1(t)\rangle_n &= [f_1^2(t)\bar{n}_1 + f_2^2(t)\bar{n}_2][f_3^2(t+\tau)(\bar{n}_3+1)\\ &+ f_4^2(t+\tau)(\bar{n}_4+1)] + \bar{n}_1\bar{n}_2[f_1(t)f_1(t+\tau) + f_2(t)f_2(t+\tau)]^2\\ &+ f_1^2(t)f_1^2(t+\tau)\bar{n}_1(\bar{n}_1-1) + f_2^2(t)f_2^2(t+\tau)\bar{n}_2(\bar{n}_2+1)\\ &+ 2[f_1(t)f_1(t+\tau)\bar{n}_1 + f_2(t)f_2(t+\tau)\bar{n}_2][f_3(t)f_3(t+\tau)(\bar{n}_3+1)\\ &+ f_4(t)f_4(t+\tau)(\bar{n}_4+1)]\\ &+ [f_1^2(t+\tau)\bar{n}_1 + f_2^2(t+\tau)\bar{n}_2][f_3^2(t)(\bar{n}_3+1) + f_4^2(t)(\bar{n}_4+1)]\\ &+ (\bar{n}_3+1)(\bar{n}_4+1)[f_3(t)f_4(t+\tau) + f_4(t)f_3(t+\tau)]^2\\ &+ f_3^2(t)f_3^2(t+\tau)(\bar{n}_3+1)(\bar{n}_3+2) + f_4^2(t)f_4^2(t+\tau)(\bar{n}_4+1)(\bar{n}_4+2)\end{aligned} \tag{4.5a}$$

$$\begin{aligned}\langle \hat{a}_3^\dagger(t)\hat{a}_3^\dagger(t+\tau)\hat{a}_3(t+\tau)\hat{a}_3(t)\rangle_n &= [h_3^2(t)\bar{n}_3 + h_4^2(t)\bar{n}_4][h_2^2(t+\tau)(\bar{n}_2+1)\\ &+ h_1^2(t+\tau)(\bar{n}_1+1)] + \bar{n}_3\bar{n}_4[h_3(t)h_4(t+\tau) + h_4(t)h_3(t+\tau)]^2\\ &+ h_3^2(t)h_3^2(t+\tau)\bar{n}_3(\bar{n}_3-1) + h_4^2(t)h_4^2(t+\tau)\bar{n}_4(\bar{n}_4+1)\\ &+ 2[h_3(t)h_3(t+\tau)\bar{n}_3 + h_4(t)h_4(t+\tau)\bar{n}_4]\\ &\times [h_2(t)h_2(t+\tau)(\bar{n}_1+1) + h_1(t)h_1(t+\tau)(\bar{n}_1+1)]\\ &+ [h_3^2(t+\tau)\bar{n}_3 + h_4^2(t+\tau)\bar{n}_4][h_1^2(t)(\bar{n}_1+1) + h_2^2(t)(\bar{n}_2+1)]\\ &+ (\bar{n}_2+1)(\bar{n}_2+1)[h_1(t)h_2(t+\tau) + h_2(t)h_1(t+\tau)]^2\\ &+ h_1^2(t)h_1^2(t+\tau)(\bar{n}_1+1)(\bar{n}_1+2) + h_2^2(t)h_2^2(t+\tau)(\bar{n}_2+1)(\bar{n}_2+2).\end{aligned} \tag{4.5b}$$

Firstly, we will discuss the sub-Poissonian statistics, i.e. we take $\tau = 0$ in equations (4.4) and (4.5). For $n_j = 0$, i.e. for input vacuum states, we can get

$$\begin{aligned}\langle(\triangle\hat{n}_1(t))^2\rangle_0 - \langle\hat{n}_1(t)\rangle_0 &= (f_3^2(t) + f_4^2(t))^2\\ \langle(\triangle\hat{n}_3(t))^2\rangle_0 - \langle\hat{n}_3(t)\rangle_0 &= (h_1^2(t) + h_2^2(t))^2\end{aligned} \tag{4.6}$$

where the relation

$$\langle(\triangle\hat{n}_j(t))^2\rangle - \langle\hat{n}_j(t)\rangle = \langle\hat{a}_j^{\dagger 2}(t)\hat{a}_j^2(t)\rangle - \langle\hat{a}_j^\dagger(t)\hat{a}_j(t)\rangle^2 \tag{4.7}$$

has been used. It is clear from (4.6) that input vacuum states, which have maximum pronounced sub-Poissonian statistics, evolve into pure super-Poissonian statistics states for all times $t \neq 0$ inside the coupler. We display the second-order correlation function (4.1) against time t in figure 3 for input number states with different mean photon numbers $\bar{n}_j$ ($\bar{n}_1 = 4, \bar{n}_j = 1, j = 2, 3, 4$) and for different values of coupling constants. In figure 3(*a*), $g_1^{(2)}(t)$ for mode 1 is shown, where always $\lambda_2 = 1.2$, $\lambda_3 = 0.5$. $\lambda_1 = 0.1, 0.6$, corresponding to curve *A* and curve *B*, respectively. Initially, $g_1^{(2)}(0) = \frac{3}{4}$, which is the corresponding value for the Fock state $|4\rangle$. Increasing the time, switching between modes starts (see curve *A*); $g_1^{(2)}(t)$ has an oscillating behaviour between values for sub-Poissonian and super-Poissonian

statistics for rather short interaction times. However, for large interaction times the oscillations are successively washed out and super-Poissonian statistics are dominant. As seen in curve *B*, $g_1^{(2)}(t)$ does not exhibit any periodic behaviour and takes values corresponding to super-Poissonian statistics shortly after the switching on of the interaction. On the other hand, we can see that strongly sub-Poissonian light is generated not only for short-time interaction but also for larger times as demonstrated by the behaviour of $g_2^{(2)}(t)$ in the second mode for the same values of $\bar{n}_j$ as in the former case and for $(\lambda_1, \lambda_2, \lambda_3) = (0.1, 1.2, 0.5)$, see figure 3(*b*). Moreover, $g_2^{(2)}(t)$ behaves more smoothly than $g_1^{(2)}(t)$ for the same values of $\bar{n}_j$ and λ_j.

We note that for λ_2 less than λ_1 and λ_3 and $t \neq 0$, the second-order correlation functions always exhibit super-Poissonian statistics and there is no oscillatory behaviour regardless of the values of input mean photon numbers, since all time-dependent functions in equations (4.4) and (4.5) are hyperbolic functions.

For input coherent states, we have

$$\langle \hat{n}_1(t+\tau)\rangle_{coh} = |\alpha_1^* f_1(t+\tau) - \mathrm{i}\alpha_2^* f_2(t+\tau) + \mathrm{i}\alpha_3 f_3(t+\tau) + \alpha_4 f_4(t+\tau)|^2 + f_3^2(t+\tau) + f_4^2(t+\tau) \tag{4.8a}$$

$$\langle \hat{n}_3(t+\tau)\rangle_{coh} = |\alpha_3 h_3(t+\tau) - \mathrm{i}\alpha_1^* h_1(t+\tau) + \alpha_2^* h_2(t+\tau) - \mathrm{i}\alpha_4 h_4(t+\tau)|^2 + h_1^2(t+\tau) + h_2^2(t+\tau) \tag{4.8b}$$

$$\langle \hat{a}_1^\dagger(t)\hat{a}_1^\dagger(t+\tau)\hat{a}_1(t+\tau)\hat{a}_1(t)\rangle_{coh} = \langle \hat{n}_1(t)\rangle_{coh}\langle \hat{n}_1(t+\tau)\rangle_{coh} + [f_3(t)f_3(t+\tau) + f_4(t)f_4(t+\tau)]^2 + [f_3(t)f_3(t+\tau) + f_4(t)f_4(t+\tau)][\langle \hat{a}_1^\dagger(t)\rangle_{coh}\langle \hat{a}_1(t+\tau)\rangle_{coh} + \text{c.c.}] \tag{4.9a}$$

$$\langle \hat{a}_3^\dagger(t)\hat{a}_3^\dagger(t+\tau)\hat{a}_3(t+\tau)\hat{a}_3(t)\rangle_{coh} = \langle \hat{n}_3(t)\rangle_{coh}\langle \hat{n}_3(t+\tau)\rangle_{coh} + [h_1(t)h_1(t+\tau) + h_2(t)h_2(t+\tau)]^2 + [h_1(t)h_1(t+\tau) + h_2(t)h_2(t+\tau)][\langle \hat{a}_3^\dagger(t)\rangle_{coh}\langle \hat{a}_3(t+\tau)\rangle_{coh} + \text{c.c.}] \tag{4.9b}$$

where $\langle \hat{n}_j(t)\rangle_{coh}$ can be obtained from $\langle \hat{n}_j(t+\tau)\rangle_{coh}$ by simply setting $\tau = 0$; $\langle \hat{a}_j(t)\rangle_{coh}$ is the expectation value for $\hat{a}_j(t)$ in the coherent states and c.c. is the complex conjugate.

From equations (4.1) it is clear that the condition for sub-Poissonian statistics is that the variance $\langle(\triangle\hat{n}_j(t))^2\rangle$ is less that the mean photon number $\langle \hat{n}_j(t)\rangle$. Combining (4.8) and (4.9) into (4.7), after taking $\tau = 0$, it is easy to show that this system cannot provide sub-Poissonian light for input coherent light. For instance, for mode 1, from equations (4.7) with (4.8*a*), (4.9*a*) it follows that sub-Poissonian light could be generated provided that

$$2|\alpha_1^* f_1(t) - \mathrm{i}\alpha_2^* f_2(t) + \mathrm{i}\alpha_3 f_3(t) + \alpha_4 f_4(t)|^2 + f_3^2(t) + f_4^2(t) < 0. \tag{4.10}$$

It is evident that this inequality cannot be fulfilled regardless of the values of α_j and λ_j. More precisely, for input coherent light, this model can generate classical light, e.g. coherent, partially coherent and chaotic light.

In figures 4 and 5 we have plotted $g_j^{(2)}(t)$ against time t for $\lambda_1 = 0.1$, $\lambda_2 = 1.2$, $\lambda_3 = 0.5$ and input coherent light with complex amplitudes $\alpha_j = |\alpha_j|\mathrm{e}^{\psi_j}$. In all these figures $g_j^{(2)}(0) = 1$ initially. In figure 4, for $|\alpha_j| = 1$ and $(\psi_1, \psi_2, \psi_3, \psi_4) = (\frac{\pi}{2}, \frac{\pi}{3}, \frac{\pi}{3}, \frac{\pi}{3})$, we see the oscillatory behaviour in the evolution of $g_j^{(2)}(t)$ in all cases showing that the photons are transferred from one mode to the other. These oscillations successively disappear for large interaction times. They can be destroyed by changing the values of the complex amplitudes of input light, but not by changing the values of the coupling constants (see figure 5 for shown values). This shows how one can control light by light via nonlinear medium. In figure 5(*a*) we can see the periodic behaviour exhibiting photon statistics between almost Poissonian and super-Poissonian ones for mode 1 with gradual increase of values of $g^{(2)}(t) = 2$ representing chaotic light for larger

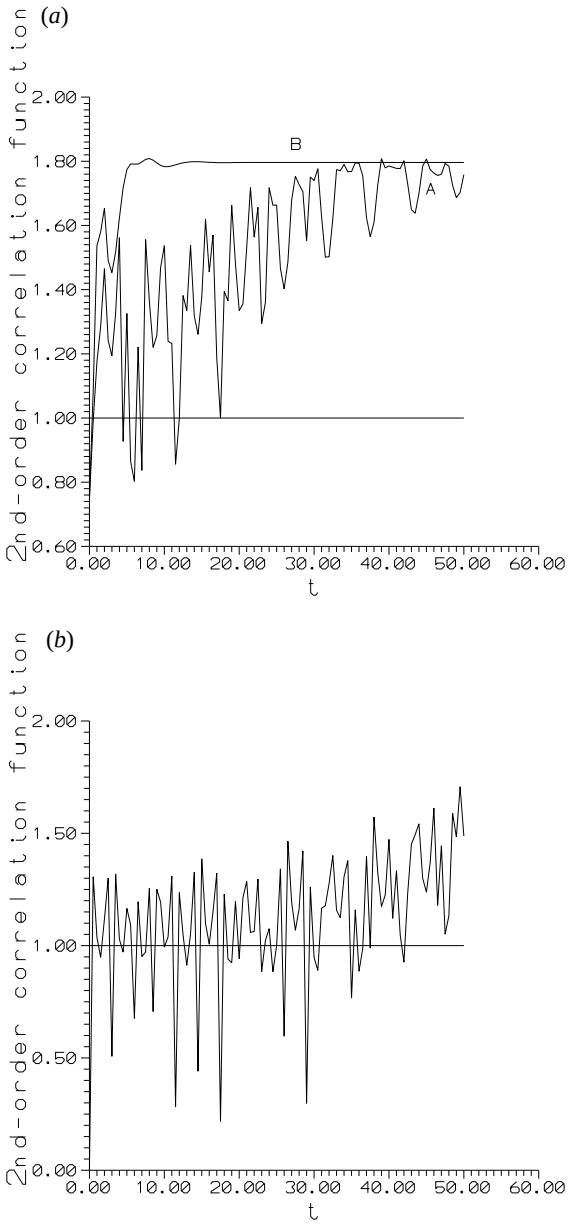

Figure 3. Normalized normal second-order correlation function when both the modes are initially in the number states with mean photon number $\bar{n}_1 = 4, \bar{n}_j = 1, j = 2, 3, 4$. For all curves $\lambda_2 = 1.2$ and $\lambda_3 = 0.5$. For curve A, $\lambda_1 = 0.1$ and for curve B, $\lambda_1 = 0.6$: (*a*) $g_1^{(2)}(t)$ for mode 1; (*b*) $g_2^{(2)}(t)$ for mode 2. The full line corresponds to $g^{(2)}(0)$ of the coherent light.

interaction times. We see that the initial coherent state can be successively approximately regenerated. From figure 5(*b*) we can see that the precise Poisson distribution is obtained only initially and partially coherent light is obtained for later times, with the maximal noise value in mode 3 (curve B). For input coherent light $1 \preceq g_j^{(2)}(t) \preceq 2$ holds, i.e. one cannot obtain

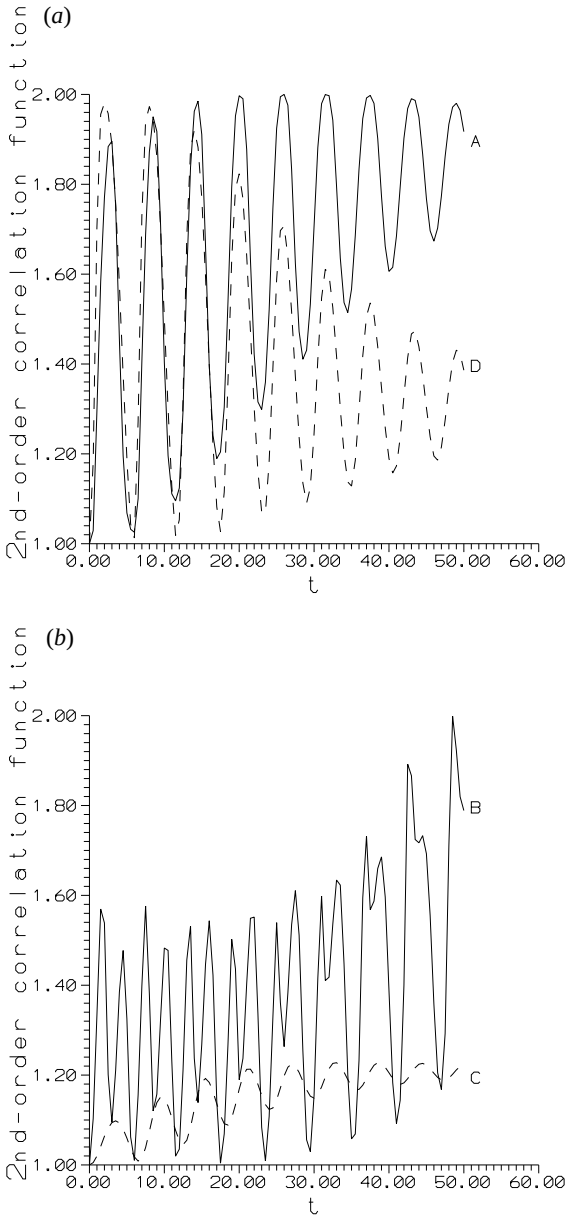

Figure 4. Normalized normal second-order correlation function $g_j^{(2)}(t)$ for different modes when both the modes are initially in the coherent states with $|\alpha_j| = 1$, $j = 1, 2, 3, 4$, $\psi_1 = \frac{\pi}{2}$ and $\psi_j = \frac{\pi}{3}$, $j = 2, 3, 4$ for all curves, $\lambda_1 = 0.1$, $\lambda_2 = 1.2$ and $\lambda_3 = 0.5$: (*a*) first mode, curve A, and fourth mode, curve D; (*b*) second mode, curve B, and third mode, curve C.

superchaotic light. One can also observe some complementary behaviour of both the modes.

Concerning photon bunching and antibunching according to the definition (4.3), we have analysed the cases of input number and coherent states. We note, in general, that the quantity $K_j(t)$ exhibits oscillatory behaviour between negative and positive values for both number and coherent input states, i.e. both antibunching and bunching can occur. The photon antibunching

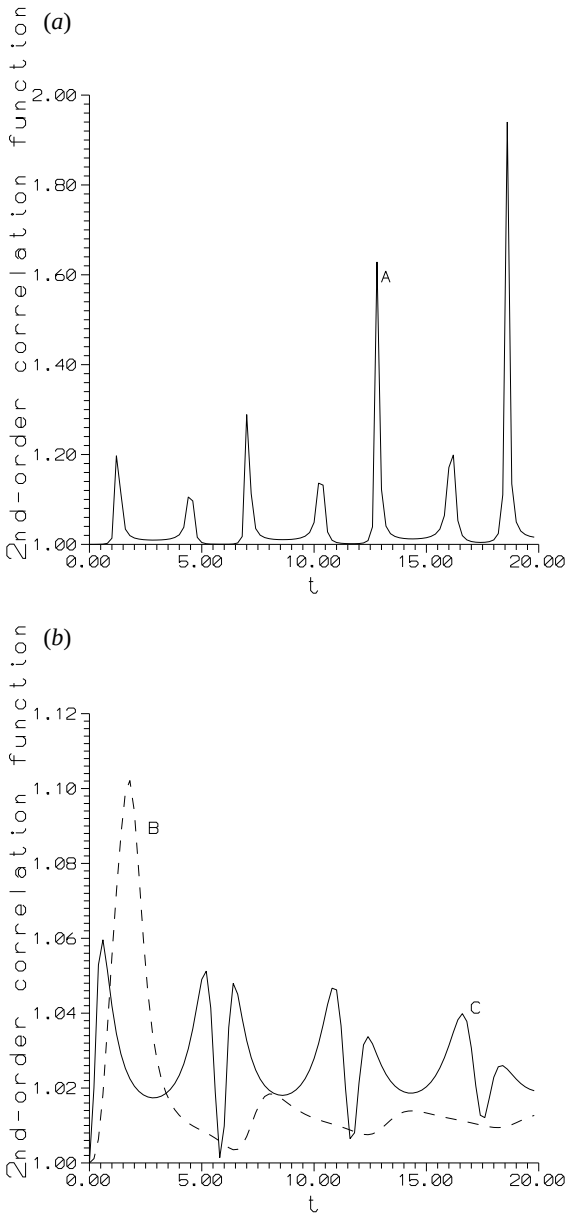

Figure 5. Normalized normal second-order correlation function $g_j^{(2)}(t)$ for different modes when both the modes are initially in the coherent states with $|\alpha_1| = 10, |\alpha_j| = 1, j = 2, 3, 4$, $\psi_j = \frac{\pi}{6}, j = 1, 2, 3, 4$ where λ_j have the same values as in figure 4: (*a*) first mode; (*b*) third mode, curve B, and fourth mode, curve C.

is more pronounced for input number states than for input coherent states. Comparing these results with those for sub-Poisson statistics, we can conclude that there is no direct relation between antibunching and sub-Poissonian statistics here, in agreement with results shown in the literature [37, 38]. We can demonstrate this graphically in figure 6, by considering the first mode, for input number state (solid curve) and for input coherent state (centred curve) for

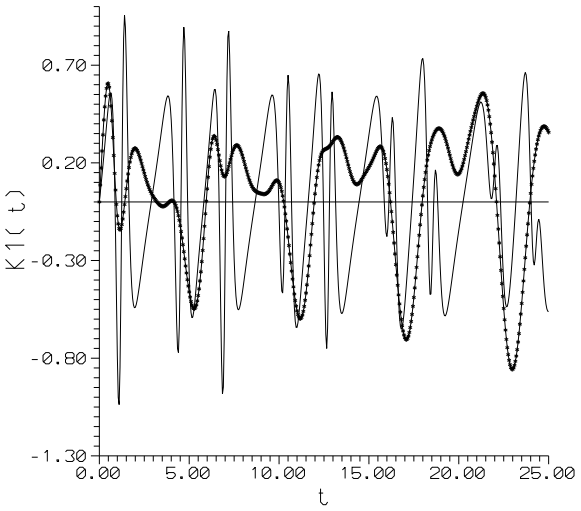

Figure 6. The quantity $K_1(t)$ for mode 1 when both the modes are initially in the number (solid curve) and coherent (centred curve) input states for the same situation as in figure 3(*a*) (curve A) and figure 4(*a*) for number state and coherent state, respectively.

the same values of parameters as those of figures 3(*a*) (curve A) and 4(*a*). It is interesting to mention that three definitions of photon antibunching can be given, which are not equivalent for nonstationary fields and the problem is still under consideration by some authors [39].

We conclude this section by turning our attention to the cross-correlation between different modes in the model. Cross-correlation may be used to describe anticorrelation between modes, which may cause the variance of the photon number to be less than the average of the photon number, thus causing antibunching, and it can be measured by detecting single modes separately by two photodetectors and correlating their outputs. Cross-correlation between jth mode and kth mode is controlled by

$$\triangle_{cross}^{(j,k)} = \langle \hat{a}_j^\dagger(t)\hat{a}_j(t)\hat{a}_k^\dagger(t)\hat{a}_k(t)\rangle - \langle \hat{a}_j^\dagger(t)\hat{a}_j(t)\rangle\langle \hat{a}_k^\dagger(t)\hat{a}_k(t)\rangle \qquad j \neq k. \tag{4.11}$$

When the initial input states are coherent states, we find

$$\triangle_{cross}^{(1,2)} = \mathrm{i}(f_1(t)g_1(t) + f_2(t)g_2(t))(\bar{\alpha}_1^*(t)\bar{\alpha}_2(t) - \bar{\alpha}_1(t)\bar{\alpha}_2^*(t)) + (f_1(t)g_1(t) + f_2(t)g_2(t))^2 \tag{4.12a}$$

$$\triangle_{cross}^{(1,3)} = \mathrm{i}(f_3(t)h_3(t) + f_4(t)h_4(t))(\bar{\alpha}_1(t)\bar{\alpha}_3(t) - \bar{\alpha}_1^*(t)\bar{\alpha}_3^*(t)) + (f_3(t)h_3(t) + f_4(t)h_4(t))^2 \tag{4.12b}$$

$$\triangle_{cross}^{(3,4)} = \mathrm{i}(l_3(t)h_3(t) - l_4(t)h_4(t))(\bar{\alpha}_3^*(t)\bar{\alpha}_4(t) - \bar{\alpha}_3(t)\bar{\alpha}_4^*(t)) + (h_3(t)l_3(t) - l_4(t)h_4(t))^2 \tag{4.12c}$$

where $\bar{\alpha}_j(t)$ are the mean values of the operators $\hat{a}_j(t)$ with respect to coherent states, given by equations (4.5). In figure 7, we have plotted evolution of cross-correlation functions given by (4.12) against time t for input coherent light having amplitudes $|\alpha_j|^2 = 2$ and coupling constants λ_j have the same values as those in figure 4. It is evident that anticorrelation occurs in all cases. The cross-correlations between signal and idler modes in the same waveguide (curves B and F) exhibit oscillatory behaviour with time. Also, we can see that the values in the second waveguide (curve F) are more pronounced than in the first waveguide (curve B) owing to $\lambda_3 > \lambda_1$. Minimum cross-correlation is reached between idler modes (3, 4) (curve E).

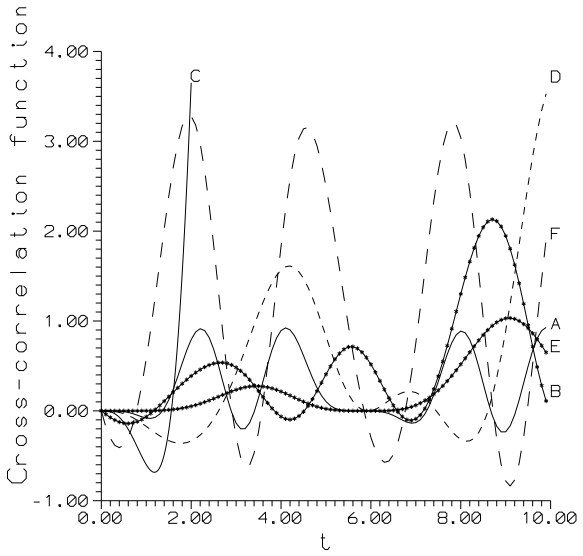

Figure 7. Cross-correlation function for different modes when all modes are initially in the coherent states with $|\alpha_j|^2 = 2$, where λ_j have the same values as in figure 4. Curves A–F represent correlation between modes (1, 2), (1, 3), (1, 4), (2, 3), (3, 4) and (4, 2), respectively.

5. Quasiprobability functions

The important quantities in quantum mechanics are the different moments for the harmonic oscillator. Such moments are the basis to study the quantum statistical properties of quantum system. There are two ways for obtaining a more complete statistical description of the field based on characteristic functions and quasiprobability distribution functions. In this section we study such functions for the model under discussion. For this model we consider joint quasiprobability functions as well as the single-mode quasiprobability function for two cases when all modes enter the coupler in coherent states as well as in number states.

As is well known, the single-mode s-parametrized characteristic function is defined as

$$C^{(1)}(\zeta_j, s, t) = \mathrm{Tr}\left[\hat{\rho}(0)\exp\left(\frac{s}{2}|\zeta_j|^2 + \zeta_j\hat{a}_j^\dagger(t) - \zeta_j^*\hat{a}_j(t)\right)\right] \tag{5.1}$$

where s takes on values 1, 0 and -1 corresponding to normally, symmetrically and antinormally ordered characteristic functions, respectively. $\hat{\rho}(0)$ is the initial density operator for the system, Tr denotes trace of the operator and $j = 1, 2, 3, 4$.

The single-mode s-parametrized quasiprobability distribution functions are formally defined by the Fourier transform of the s-parametrized characteristic functions as

$$W^{(1)}(\alpha_j, s, t) = \frac{1}{\pi^2}\int \mathrm{d}^2\zeta_j\, C^{(1)}(\zeta_j, s, t)\exp(\alpha_j\zeta_j^* - \zeta_j\alpha_j^*). \tag{5.2}$$

Now we extend the definitions of the single-mode characteristic function and single-mode quasiprobability functions to include four modes (joint quasiprobability functions), as

$$C^{(4)}(\underline{\zeta}, s, t) = \mathrm{Tr}\left[\hat{\rho}(0)\exp\sum_{i=1}^{4}\left(\frac{s}{2}|\zeta_i|^2 + \zeta_i\hat{a}_i^\dagger(t) - \zeta_i^*\hat{a}_i(t)\right)\right] \tag{5.3}$$

$$W^{(4)}(\underline{\alpha}, s, t) = \frac{1}{\pi^8}\int C^{(4)}(\underline{\zeta}, s, t)\prod_{j=1}^{4}\exp[(\alpha_j\zeta_j^* - \alpha_j^*\zeta_j)]\,\mathrm{d}^2\zeta_j \tag{5.4}$$

where $C^{(4)}(\underline{\zeta}, s, t)$ is given by (5.3). When $s = 1, 0, -1$, equation (5.4) gives formally a Glauber P-function, Wigner W-function and Husimi Q-function, respectively. For the sake of simplicity, we have used the notations $\underline{\alpha} = (\alpha_1, \alpha_2, \alpha_3, \alpha_4)$ and $\underline{\zeta} = (\zeta_1, \zeta_2, \zeta_3, \zeta_4)$.

The superscripts (1) and (4) in the above equations stand for single-mode case and four-mode case, respectively.

The known relations for the different moments of the bosonic operators for the single mode in terms of characteristic functions and quasiprobability functions [40] can be extend to four modes. In other words, the normal form, antinormal form and symmetrical form for moments of bosonic operators for four modes can be evaluated with the help of the joint charateristic functions by differentiation or by integration using joint quasiprobability functions as

$$\left\langle \prod_{j=1}^{4} \hat{a}_j^{\dagger m_j}(t)\hat{a}_j^{n_j}(t) \right\rangle = \prod_{j=1}^{4} \frac{\partial^{m_j+n_j}}{\partial \zeta_j^{m_j} \partial(-\zeta_j^*)^{n_j}} C^{(4)}(\underline{\zeta}, s=1, t)|_{\underline{\zeta}=\underline{\zeta}^*=0}$$

$$= \int W^{(4)}(\underline{\alpha}, s=1, t) \prod_{j=1}^{4} \alpha_j^{*m_j} \alpha_j^{n_j} \, \mathrm{d}^2\alpha_j \tag{5.5}$$

$$\left\langle \prod_{j=1}^{4} \hat{a}_j^{m_j}(t)\hat{a}_j^{\dagger n_j}(t) \right\rangle = \prod_{j=1}^{4} \frac{\partial^{m_j+n_j}}{\partial \zeta_j^{n_j} \partial(-\zeta_j^*)^{m_j}} C^{(4)}(\underline{\zeta}, s=-1, t)|_{\underline{\zeta}=\underline{\zeta}^*0}$$

$$= \int W^{(4)}(\underline{\alpha}, s=-1, t) \prod_{j=1}^{4} \alpha_j^{*n_j} \alpha_j^{m_j} \, \mathrm{d}^2\alpha_j \tag{5.6}$$

$$\left\langle \prod_{j=1}^{4} \hat{a}_j^{\dagger m_j}(t)\hat{a}_j^{n_j}(t) \right\rangle = \prod_{j=1}^{4} \frac{\partial^{m_j+n_j}}{\partial \zeta_j^{m_j} \partial(-\zeta_j^*)^{n_j}} C^{(4)}(\underline{\zeta}, s=0, t)|_{\underline{\zeta}=\underline{\zeta}^*=0}$$

$$= \int W^{(4)}(\underline{\alpha}, s=0, t) \prod_{j=1}^{4} \alpha_j^{*m_j} \alpha_j^{n_j} \, \mathrm{d}^2\alpha_j \tag{5.7}$$

where n_j, m_j are positive integers, and $\int$ is multi-integral over $\alpha_1, \alpha_2, \alpha_3, \alpha_4$ phase space. It is known that P-representation is sometimes difficult to use, for instance in interaction problems, since it can be highly singular.

5.1. Input coherent light

Now we turn our attention to calculation of the previous quantities when the initial input light is coherent. The density operator is

$$\hat{\rho}_{coh}(0) = \prod_{j=1}^{4} |\alpha\rangle_{\mathrm{jj}}\langle\alpha|. \tag{5.8}$$

and for the joint s-parametrized characteristic function we have

$$C_{coh}^{(4)}(\underline{\zeta}, s, t) = \exp \sum_{j=1}^{4} [\tfrac{1}{2}(s|\zeta_j|^2 - |\eta_j(t)|^2) + (\bar{\alpha}_j^*(t)\zeta_j - \bar{\alpha}_j(t)\zeta_j^*)] \tag{5.9}$$

where $\bar{\alpha}_j(t)$ are the mean values of the operators $\hat{a}_j(t)$ with respect to the coherent states and $\eta_j(t)$, $j = 1, 2, 3, 4$ are given by

$$\eta_1(t) = \zeta_1 f_1(t) + \mathrm{i}\zeta_2 g_1(t) + \mathrm{i}\zeta_3^* h_1(t) - \zeta_4^* l_1(t) \tag{5.10a}$$

$$\eta_2(t) = \zeta_2 g_2(t) - \mathrm{i}\zeta_1 f_2(t) + \mathrm{i}\zeta_4^* l_2(t) - \zeta_3^* h_2(t) \tag{5.10b}$$

$$\eta_3(t) = \zeta_3 h_3(t) + \mathrm{i}\zeta_1^* f_3(t) - \zeta_2^* g_3(t) + \mathrm{i}\zeta_4 l_3(t) \tag{5.10c}$$

$$\eta_4(t) = \zeta_4 l_4(t) + \mathrm{i}\zeta_3 h_4(t) + \mathrm{i}\zeta_2^* g_4(t) - \zeta_1^* f_4(t). \tag{5.10d}$$

Equations (5.4) and (5.9) lead to the joint Wigner function expressed as

$$W^{(4)}(\underline{\alpha}, s=0, t) = \frac{16}{\pi^4} \exp\left(-2 \sum_{j=1}^{4} |\chi_j(t)|^2 \right) \tag{5.11}$$

where

$$\chi_1(t) = \mu_1(t) f_1(t) + \mathrm{i}\mu_2(t) g_1(t) + \mathrm{i}\mu_3^*(t) h_1(t) - \mu_4^*(t) l_1(t) \tag{5.12a}$$

$$\chi_3(t) = \mathrm{i}\mu_1^*(t) f_3(t) - \mu_2^*(t) g_3(t) + \mu_3(t) h_3(t) + \mathrm{i}\mu_4(t) l_3(t) \tag{5.12b}$$

$\mu_j(t) = \bar{\alpha}_j(t) - \alpha_j$, and $\chi_2(t)$, $\chi_4(t)$ can be obtained with the aid of transformation (2.8).

The expression for the joint Q-function is obtained in appendix A.

The single-mode s-parametrized characteristic function and s-parametrized quasiprobability function are given, respectively, as

$$C^{(1)}(\zeta_j, s, t) = \exp\left[-\frac{|\zeta_j|^2}{2} (\tau_j^2(t) - s) + \zeta_j |\bar{\alpha}_j^*(t) - \zeta_j^* \bar{\alpha}_j(t) \right] \tag{5.13}$$

$$W^{(1)}(\alpha_j, s, t) = \frac{2}{\pi(\tau_j(t) - s)} \exp\left[-2 \frac{|\bar{\alpha}_j(t) - \alpha_j|^2}{(\tau_j(t) - s)} \right] \tag{5.14}$$

where $j = 1, 2, 3, 4$ and

$$\begin{aligned} \tau_1(t) &= f_1^2(t) + f_2^2(t) + f_3^2(t) + f_4^2(t) \\ \tau_3(t) &= h_1^2(t) + h_2^2(t) + h_3^2(t) + h_4^2(t). \end{aligned} \tag{5.15}$$

Without much effort one can see in equation (5.14) that the single-mode P-representation obtained for $s = 1$ has δ-function singularity only at $t = 0$, i.e. for the coherent state. In other words, with respect to switching between modes inside the coupler this singularity is washed out. On the other hand, the joint Wigner function has time-dependent Gaussian forms. In fact, the Gaussian property of the joint Wigner function has been used earlier to establish the higher-order squeezing [41] properties of four-wave mixing [42]: if a field is squeezed to the second order then it will be squeezed to all even orders. A similar property was proved in the context of interferometers [43]. Also we can say that even higher-order squeezing in terms of the quadratures $\hat{X}_1$ and $\hat{Y}_1$, given in section 3, can be generated in this system. For more details see [42].

Here we evaluate the joint as well as the single-mode marginal position distribution functions in terms of the Wigner function [44]. Derivation of the marginal position distribution function is given in appendix B. The single-mode marginal position distribution function can be obtained with the help of the joint marginal position distribution function (B.2), given in appendix B, by

$$P^{(1)}(x_{s1}, t) = \int_{-\infty}^{\infty} \int_{-\infty}^{\infty} \int_{-\infty}^{\infty} P^{(4)}(\underline{x}, t)\, \mathrm{d}x_{s2}\, \mathrm{d}x_{s3}\, \mathrm{d}x_{s4} \tag{5.16}$$

where sj takes on different values $1, 2, 3, 4$ in correspondence with the required mode. Therefore, we have

$$P^{(1)}(x_{s1}, t) = \frac{1}{\sqrt{\pi\, \Upsilon_{s1}(t)}} \exp\left[-\frac{[x_{s1} - \frac{1}{2}(\bar{\alpha}_1^*(t) + \bar{\alpha}_1(t))]^2}{\Upsilon_{s1}(t)} \right] \tag{5.17}$$

where $s1 = 1, 2, 3, 4$ and

$$\begin{aligned} \Upsilon_1(t) &= \tfrac{1}{2} + f_3^2(t) + f_4^2(t) \\ \Upsilon_3(t) &= \tfrac{1}{2} + h_1^2(t) + h_2^2(t) \end{aligned} \tag{5.18}$$

and $\Upsilon_{2,4}$ are obtained by substitutions (2.8). Equation (5.17) has Gaussian form with both centre and width being time dependent.

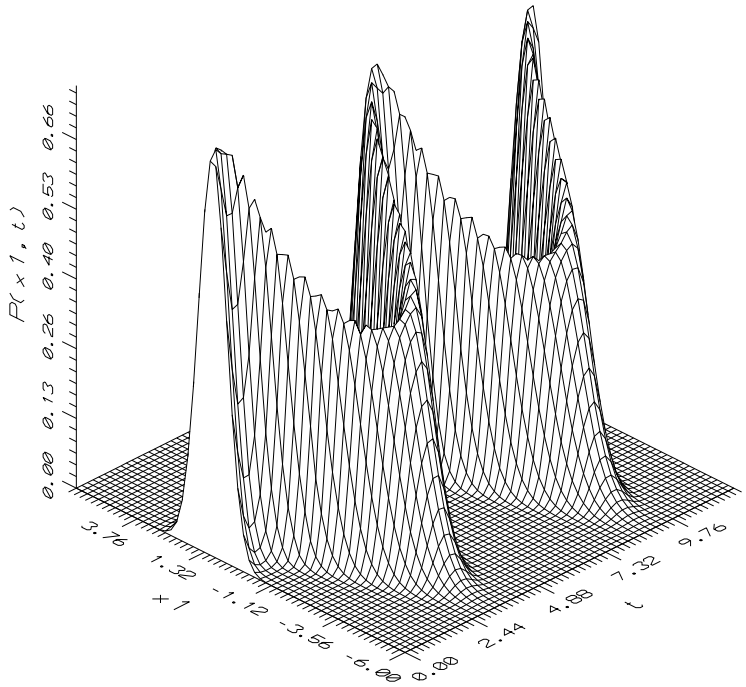

Figure 8. Quadrature distribution function $P(x_1, t)$ for the first mode against both x_1 and t for the same values of λ_j as those in figure 4 and $|\alpha_j| = \sqrt{2}$.

In figure 8 we have plotted the distribution function $P(x_1, t)$ against both x_1 and t for the same values of λ_j and $|\alpha_j|$ as those in figure 5. We can see that the distinguishable Gaussian curve for $P(x)$ for coherent state, at $t = 0$, has been evolved with time by being centre-shifted, squeezed and rotated in phase space. Moreover, we can observe the periodicity of the time-dependent functions, $f_j(t)$, in the figure, showing a complete switching of energy between modes.

5.2. Input number states

Now we discuss the previous quantities for input number states, where the density operator takes the form

$$\hat{\rho}_n(0) = \prod_{j=1}^{4} |n\rangle_{jj}\langle n|. \tag{5.19}$$

Therefore, the s-parametrized characteristic function is

$$C_n^{(4)}(\underline{\zeta}, s, t) = \prod_{j=1}^{4} \exp(-\tfrac{1}{2}|\eta_j(t)|^2) L_{n_j}(|\eta_j(t)|^2) \tag{5.20}$$

where $\eta_j(t)$ is given by (5.10) and L_n is the Laguerre polynomial of order n. The joint Wigner function is

$$W_n^{(4)}(\underline{\alpha}, t) = \frac{16}{\pi^4} \prod_{j=1}^{4} \exp(-2|\epsilon_j(t)|^2) L_{n_j}(4|\epsilon_j(t)|^2) \tag{5.21}$$

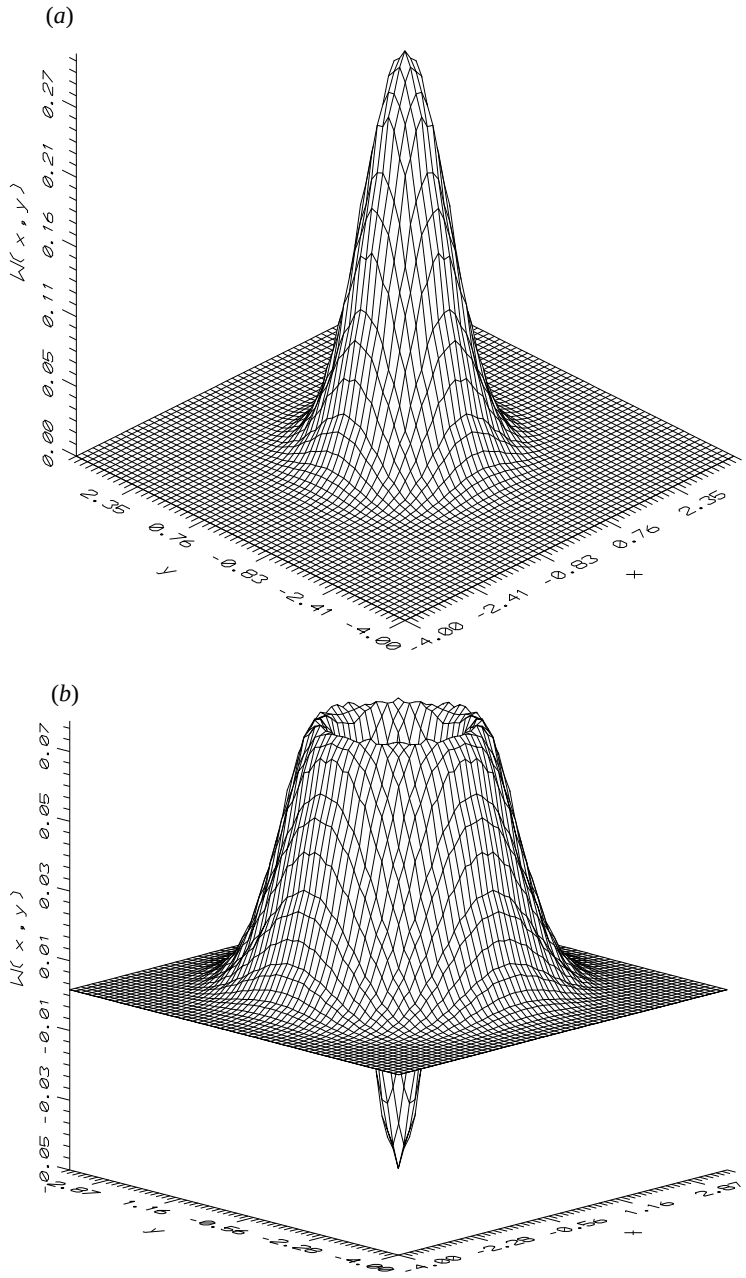

Figure 9. W-function for the single mode (mode 1) for different values of time t when initially the first mode is $|1\rangle$ and the other modes are in vacuum states $|0\rangle_j$. $|\alpha_j|^2 = 2$, and λ_k are the same as in figure 4: (*a*) for $t = \frac{\pi}{2}$; (*b*) for $t = \pi$.

where $\epsilon_j(t)$ are

$$\epsilon_1(t) = \alpha_1 f_1(t) + \mathrm{i}\alpha_2 g_1(t) + \mathrm{i}\alpha_3^* h_1(t) - \alpha_4^* l_1(t) \tag{5.22a}$$

$$\epsilon_3(t) = \alpha_3 h_3(t) + \mathrm{i}\alpha_4 l_3(t) + \mathrm{i}\alpha_1^* f_3(t) - \alpha_4^* g_3(t). \tag{5.22b}$$

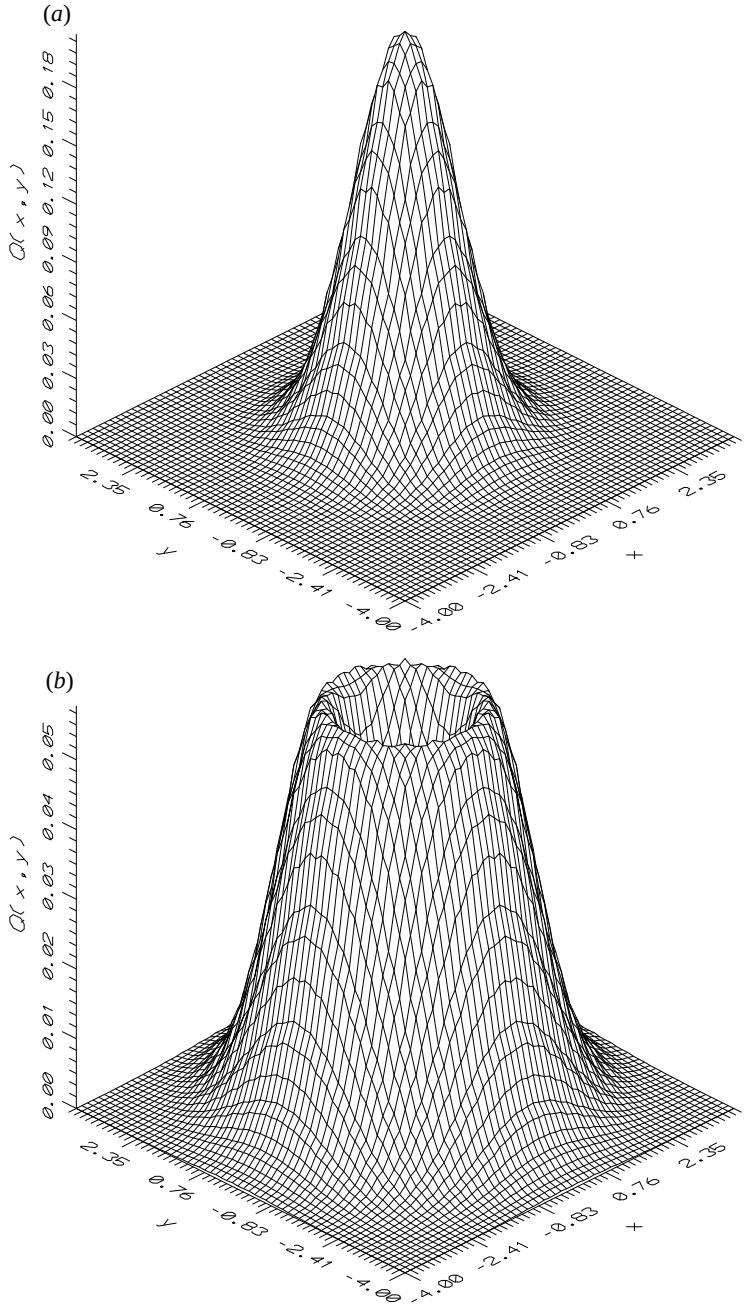

Figure 10. *Q*-function for the single mode (mode 1) for the same situation as in figure 9.

The other quantities $\epsilon_2(t)$ and $\epsilon_4(t)$ can be obtained with the help of transformation (2.8).

The single-mode s-parametrized characteristic and s-parametrized quasiprobability functions, for mode 1, can be read as

$$C_n^{(1)}(\zeta_1, s, t) = \exp\left(-\frac{|\zeta_1|}{2}(\tau_1(t) - s)\right)\prod_{j=1}^{4} L_{n_j}(|\zeta_1|^2 f_j^2(t)) \tag{5.23}$$

$$W_n^{(1)}(\alpha, t, s) = \frac{2}{\pi(\tau_1(t) - s)}\prod_{j=1}^{4} L_{n_j}\left[f_j^2(t)\frac{\partial^2}{\partial\alpha\partial(-\alpha^*)}\right]\exp\left(-\frac{2|\alpha|^2}{\tau_1(t) - s}\right). \tag{5.24}$$

Similar expressions can be obtained for the other modes by replacing $f_j^2(t)$ and $\tau_1(t)$ by the corresponding quantities, e.g. by $h_j(t)$ and $\tau_3(t)$, etc.

It has been shown for a linear directional coupler that when a number of states enter one port of the coupler and a vacuum enters the other port, an $SU(2)$ coherent state is generated at the output ports [45]. The same authors have also shown that under particular conditions the linear directional coupler can serve as a generator of a displaced number state [45]. In fact, we noted for our structure that when the first mode enters the coupler in the Fock state $|1\rangle$ and the other modes enter it in vacuum states, coherent states can be generated as output light governed by the coupler parameters. This is demonstrated in figures 9 and 10 where a W-function and a Q-function given by (5.24) have been depicted for the interaction time $t = \frac{\pi}{2}$ with coupling constants taken as those in figure 4. We can see that the W-function and Q-function have symmetric Gaussian shapes with centres slightly shifted from $(0, 0)$. The width of the Q-function is greater than that of the W-function, see figures 9(a) and 10(a). However, these characteristics are closely related to those for coherent states, i.e. our model can be used also as a generator for coherent state at this interaction time.

It is worth noting that some of the original characteristics of the input Fock state $|1\rangle$ can be recovered for large interaction time $t = \pi$. This is evident in figures 9(b) and 10(b), where the W-function has negative values, but these values are less pronounced than those for the initial Fock state, see figure 2 of [46] for comparison. The Q-function also has a hole in the top.

6. Photon-number distribution

The photon concept is an integral part of the modern description of light and can be measured by a photon detector based on the photoelectric effect.

Owing to the coupler device it could be interesting to consider a photon-number selector, due to its switching properties. So we devote this section to discuss the photon-counting distribution properties of an input radiation field prepared initially with coherent states or one mode can be in the Fock state and the remaining modes in vacuum states. We use the integral relation for the photon-counting distribution in terms of the Wigner function and Laguerre polynomials given by

$$P^{(1)}(n_j, t) = \frac{2(-1)^{n_j}}{n_j!}\int W^{(1)}(\alpha_j, t)\exp(-2|\alpha_j|^2)L_{n_j}(4|\alpha_j|^2)\,\mathrm{d}^2\alpha_j \tag{6.1}$$

where j denotes the mode under consideration and $W^{(1)}(\alpha_j, t)$, the single-mode Wigner function for initially input coherent light, is given by (5.14).

Combining equations (5.14) and (6.1), and carrying out the integration, gives

$$P^{(1)}(n_j, t) = 2\frac{(\tau_j(t) - 1)^{n_j}}{(\tau_j(t) + 1)^{n_j+1}}\exp\left[-2\frac{|\bar{\alpha_j}(t)|^2}{\tau_j(t) + 1}\right]L_{n_j}\left[4\frac{|\bar{\alpha_j}(t)|^2}{1 - \tau_j^2(t)}\right] \tag{6.2}$$

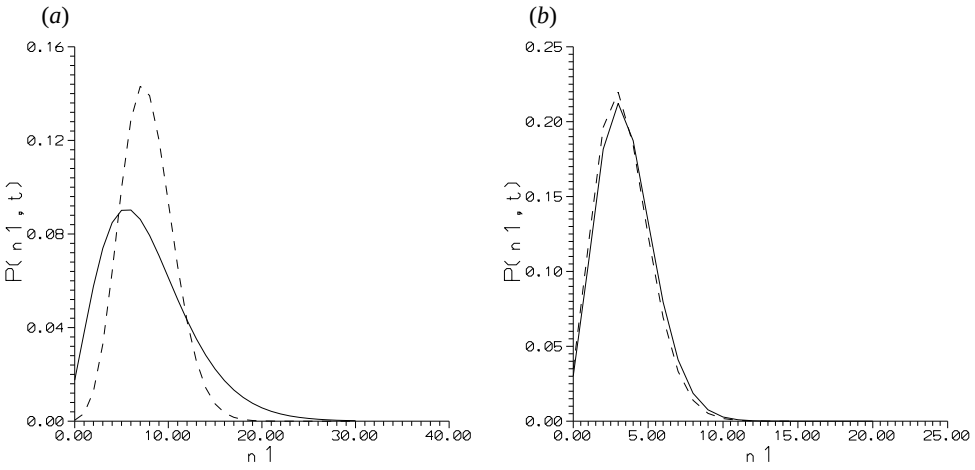

Figure 11. Photon-number distribution for the first mode $P^{(1)}(n_1, t)$ against n_1 (solid curve) for different values of time t: (*a*) λ_k are the same as in figure 4 with $t = \pi$; (*b*) $(t, \lambda_1, \lambda_2, \lambda_3) = (\frac{3\pi}{2}, 0.6, 1.6, 0.5)$; the corresponding Poisson distribution is given for comparison (dashed curve).

where $\tau_j(t)$ are given by (5.15), and $\bar{\alpha_j}(t)$, as we mentioned before, are the mean photon numbers in the jth mode with respect to coherent states.

It is easy to check that (6.2) is normalized to unity, as any probability distribution must be, i.e.

$$\sum_{n_j=0}^{\infty} P^{(1)}(n_j, t) = 1. \tag{6.3}$$

In figures 11(*a*) and (*b*) full curves represent the photon-number distribution for mode 1 for different values of time and for different values of coupling constants. In figures 11(*a*) and (*b*) we have used $(t, \lambda_1, \lambda_2, \lambda_3) = (\pi, 0.1, 1.2, 0.5)$ and $(t, \lambda_1, \lambda_2, \lambda_3) = (\frac{3\pi}{2}, 0.6, 1.6, 0.5)$, respectively. It is convenient to compare these curves with those for Poisson distribution,

$$P(n_j, t) = \frac{\langle \hat{n}_j(t) \rangle^{n_j}}{n_j!} \exp(-\langle \hat{n}_j(t) \rangle) \tag{6.4}$$

where $\langle \hat{n}_j(t) \rangle$ are given in (4.8) for $\tau = 0$, which correspond to fully coherent fields with the same $\langle \hat{n}_j(t) \rangle$. These photon distributions are shown by dashed curves. In these figures one can see that antibunching cannot occur because the actual photon distribution is broader than, or it is close to, the corresponding Poisson distribution, as shown in figures 11(*a*) and (*b*), respectively; this conclusion is in good agreement with the results of section 4.

Now we study the photon-number distribution when one mode enters the structure in number state and the other modes are in vacuum states, e.g. assuming mode 1 starts with m photons and the other modes are initially in vacuum $|0\rangle_j$. So the photon-number distribution to find n_1 photons in mode 1 can be given with the help of equation (5.24) and relation (6.1) as

$$P^{(1)}(n_1, t) = \frac{(m + n_1)!(\tau_1(t) - 1)^{n_1}[1 + \tau_1(t) - 2f_1^2(t)]^m}{n_1! m! (1 + \tau_1(t))^{m+n_1+1}} \times F\left[-m, -n_1; -m - n_1, \frac{(1 + \tau_1(t))[\tau_1(t) - 2f_1^2(t) - 1]}{(1 - \tau_1(t))[2f_1^2(t) - \tau_1(t) - 1]}\right] \tag{6.5}$$

where $F(\ldots)$ is the Gaussian hypergeometric function. From expression (6.5) it can be shown

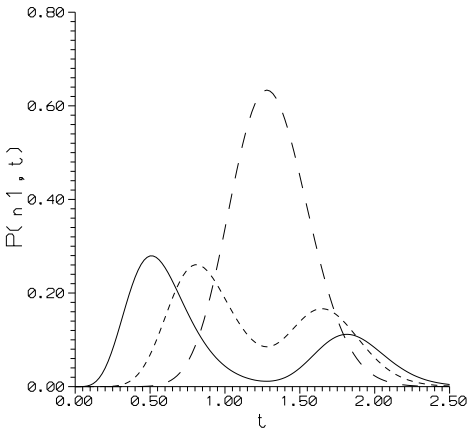

Figure 12. Photon-number distribution for mode 1 against time t, λ_j have the same values as those in figure 4 for initial input photon number $m = 6$ with different n_1: $n_1 = 4$ (solid curve), $n_1 = 2$ (small dashed curve), and $n_1 = 0$ (long dashed curve).

as a control that the initial photon-number distribution is δ_{m,n_1}, as must be. A similar expression for mode 3 can be obtained when replacing $(f_1(t), \tau_1(t), n_1)$ by $(h_3(t), \tau_3(t), n_3)$.

In figure 12 evolution of the photon-number distribution for mode 1 is plotted against time t for initial input photon number $m = 6$ with different values of n_1, and λ_j have the same values as those in figure 4. It can be seen that the nonlinear coupler acts as a selector of different photon-number distributions in the course of interaction, i.e. the maximum of probability to find, for instance, $n_1 = 2$ photons in one mode is located in a different point of the coupler with respect to the probability to find, for example, $n_1 = 4$ photons. Also we can see that the photon-number distribution for the cases $n_1 = 2, 4$ evolves into a two-peak structure, the first peak higher than the second one, and this shows that the photon-number distribution, for some cases, takes on four values for the same photon-number distribution at different intervals of the interaction time. This is in contrast to the behaviour of the photon-number distribution of a linear directional coupler [47] where the single peak structure is dominant in its behaviour.

In figure 13 the photon-number distribution is illustrated for initial photon number $m = 6$ for different modes 1, 2, 3, 4 (curves A, B, C, D, respectively) with $n_1 = 6$, $n_j = 2$, $j = 2, 3, 4$ and for shown values of λ_j. In these figures we can see some switching in terms of the photon-number distribution, based on some complementarity of photon-number distributions in various modes. For example, for short interaction times decreasing probabilities for mode 1 (curve A) gives rise to the increase of probabilities for the corresponding photon numbers of the others modes (curves B, C, D), and later on the situation is reversed, and finally the photon-number distribution in all modes is flat with negligible probabilities for single numbers.

7. Conclusions

The main conclusions of this paper are summarized as follows. Quantum statistical properties of an optical field propagating inside a directional coupler containing nondegenerate parametric amplification process have been studied in the framework of Hamiltonian formalism. Particular attention has been paid to two-mode squeezing, the second-order correlation function as well as the cross-correlation function, quasiprobability distribution functions, and photon-number distribution. Incident number states and coherent states have been considered. We have shown that for input coherent light, i.e. Poissonian light, the system can generate squeezed light in terms of two-mode squeezing depending on the values of the coupling constants. More precisely, when the linear coupling is stronger than the nonlinear one, there is the possibility to obtain squeezed light when the signal beam is in one waveguide and the idler beam in the

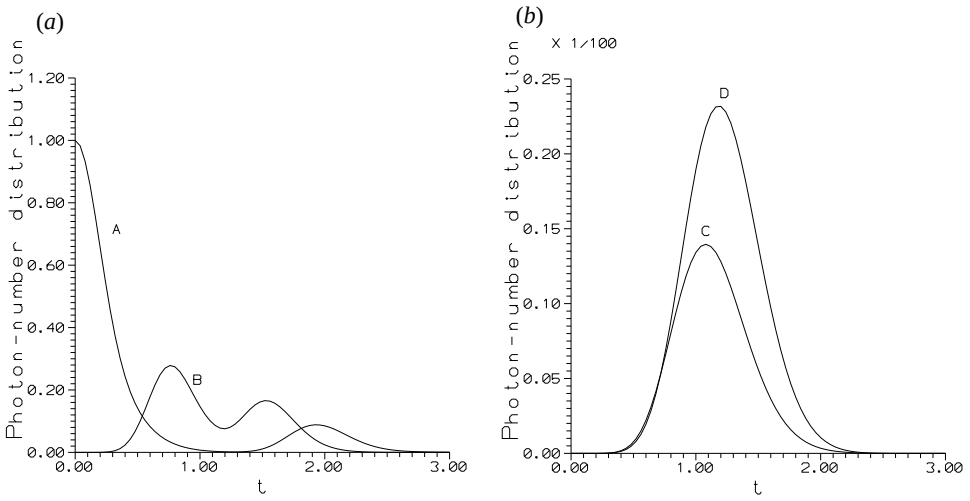

Figure 13. Photon-number distribution for initial photon number $m = 6$ for different modes 1, 2, 3, 4 with $n_1 = 6$, $n_j = 2$, $j = 2, 3, 4$ corresponding to curves A–D, respectively, for λ_j as in figure 4.

other, provided that the signal beams are connected by the evanescent waves. Nevertheless, this possibility is completely smeared when both signal or idler beams are considered. Furthermore, even higher-order squeezing can also be obtained in this system, which was exhibited in relation to the Gaussian property of the Wigner function. On the other hand, we have demonstrated that for input Fock states, i.e. for sub-Poissonian light, our model can provide sub-Poissonian light governed by coupler parameters. However, for input coherent light, coherent light, partially coherent light and chaotic light can be generated. This was demonstrated in terms of both the second-order correlation function and photon-number distribution. Concerning photon antibunching, we have shown for both number and coherent input states that the outgoing field oscillates between bunching and antibunching giving a good indication that there is no direct relation between sub-Poissonian statistics and photon antibunching, as shown in the literature previously [37, 38]. Finally, it is important to mention that the coherent state can be generated as output light from the structure under consideration when one of the input modes is in Fock state $|1\rangle$ and the other modes are in vacuum states with some control of the parameters of the coupler.

Acknowledgments

JP and FAAE-O acknowledge the partial support from Project VS96028 of the Czech Ministry of Education and from Project 202/96/0421 of the Czech Grant Agency. MSA is grateful to Professor B E Saleh from the Electrical Engineering Department, University of Boston, where part of this work has been achieved, for his hospitality. MSA is also grateful for financial support from the project Math 1418/19 of the Research Centre, College of Science, King Saud University.

Appendix A

In this appendix we write the exact form for the joint Q-function. It can be calculated similarly as the joint Wigner function by inserting the joint antinormal characteristic function given by (5.8) into (5.2) and carrying out the integration. We get, after tedious calculation, that

$$Q^{(4)}(\underline{\alpha},t)=\frac{(1-R_4^2(t))}{\pi^4 S_1(t)S_2(t)S_3(t)S_4(t)}[K_1(t)K_2(t)-J^2(t)]^{-1}\times\exp\left(-\left[|\varpi_1(t)|^2+\frac{|\varpi_2(t)+\mathrm{i}R_4(t)\varpi_1(t)|^2}{1-R_4^2(t)}+\frac{|U(t)|^2}{K_1(t)(1-R_4^2(t))}\right]\right)\times\exp\left(-\frac{K_1(t)Z^2(t)}{(K_1(t)K_2(t)-J^2(t))(1-R_4^2(t))}\right)\tag{A.1}$$

where

$$\varpi_j(t)=\frac{\chi_j(t)}{\sqrt{S_j(t)}}\qquad j=1,2,3,4\tag{A.2a}$$

and

$$\begin{aligned}S_1(t)&=f_1^2(t)+g_1^2(t)\qquad S_2(t)=f_2^2(t)+g_2^2(t)\\S_3(t)&=h_3^2(t)+l_3^2(t)\qquad S_4(t)=h_4^2(t)+l_4^2(t)\end{aligned}\tag{A.2b}$$

$$\begin{aligned}R_1(t)&=\frac{h_2(t)h_3(t)+l_2(t)l_3(t)}{\sqrt{S_2(t)S_3(t)}}\qquad R_2(t)=\frac{f_1(t)f_4(t)+g_1(t)g_4(t)}{\sqrt{S_1(t)S_4(t)}}\\R_3(t)&=\frac{f_3(t)f_4(t)-g_3(t)g_4(t)}{\sqrt{S_3(t)S_4(t)}}\qquad R_4(t)=\frac{f_1(t)f_2(t)+g_1(t)g_2(t)}{\sqrt{S_1(t)S_2(t)}}\\R_5(t)&=\frac{g_1(t)g_3(t)-f_1(t)f_3(t)}{\sqrt{S_1(t)S_3(t)}}\qquad R_6(t)=\frac{f_2(t)f_4(t)+g_2(t)g_4(t)}{\sqrt{S_2(t)S_4(t)}}\end{aligned}\tag{A.2c}$$

$$\begin{aligned}K_1(t)&=(1-R_5^2(t))(1-R_4^2(t))-(R_4(t)R_5(t)-R_1(t))^2\\K_2(t)&=(1-R_2^2(t))(1-R_4^2(t))-(R_4(t)R_2(t)-R_6(t))^2\end{aligned}\tag{A.2d}$$

$$U(t)=(R_5(t)R_4(t)-R_1(t))(\varpi_2^*-\mathrm{i}R_4(t)\varpi_1^*)-(1-R_4^2(t))(\varpi_3(t)+\mathrm{i}R_5(t)\varpi_1^*(t))\tag{A.2e}$$

$$J(t)=(R_4(t)R_2(t)-R_6(t))(R_5(t)R_4(t)-R_1(t))+(1-R_4^2(t))(R_2(t)R_5(t)+R_3(t))\tag{A.2f}$$

and

$$Z(t)=\left|(1-R_4^2(t))(\varpi_4(t)+R_2(t)\varpi_1^*(t))+\mathrm{i}(R_2(t)R_4(t)-R_6(t))(\varpi_2^*(t)-\mathrm{i}R_4(t)\varpi_1^*(t))+\mathrm{i}\frac{J(t)U(t)}{K_1(t)}\right|\tag{A.2g}$$

where $\chi_j(t)$ are given by (5.12).

Appendix B

In this appendix we give the exact form for joint marginal position distribution which is obtained from the joint Wigner function by

$$P^{(4)}(\underline{x},t)=\int_{-\infty}^{\infty}W^{(4)}(\underline{\alpha},s=0,t)\underline{\mathrm{d}y}\tag{B.1}$$

where $\alpha_j = x_j + y_j$; combination of equations (5.11) and (B.1), and integration, leads to

$$\begin{aligned}P^{(4)}(\underline{x},t) = {} & \frac{4}{\pi}[\beta_1(t)\beta_2(t)\beta_3(t)\beta_4(t)]^{-1} \\ & \times \exp\left\{-2\sum_{i=1}^{4}[|\nu_j(t)|^2 + x_1^2 f_j^2(t) + x_2^2 g_j^2(t) + x_3^2 h_j^2(t) + x_4^2 l_j^2(t) + x_j(t)\xi_j(t)]\right\} \\ & \times \exp\{8(h_3(t)g_3(t) - g_4(t)h_4(t))x_2x_3 + 8(f_2(t)l_2(t) + f_1(t)l_1(t))x_1x_4\} \\ & \times \exp\left\{\frac{1}{2\beta_1^2(t)}(z_1(t)\cos\bar{\theta}(t) - z_4(t)\sin\bar{\theta}(t))^2\right\} \\ & \times \exp\left\{\frac{1}{2\beta_2^2(t)}(z_4(t)\cos\bar{\theta}(t) + z_1(t)\sin\bar{\theta}(t))^2\right\} \\ & \times \exp\left\{\frac{1}{2\beta_3^2(t)}(z_3(t)\cos\bar{\phi}(t) + z_2(t)\sin\bar{\phi}(t))^2\right\} \\ & \times \exp\left\{\frac{1}{2\beta_4^2(t)}(z_2(t)\cos\bar{\phi}(t) - z_3(t)\sin\bar{\phi}(t))^2\right\} \qquad \text{(B.2)}\end{aligned}$$

where

$$z_1(t) = 4\left[(f_1(t)g_1(t) + f_2(t)g_2(t))x_2 + (f_3(t)h_3(t) + f_4(t)h_4(t))x_3 + \frac{\sigma_1(t)}{4}\right] \qquad \text{(B.3}a\text{)}$$

$$z_2(t) = 4\left[(l_2(t)g_2(t) + l_1(t)g_1(t))x_4 - (f_1(t)g_1(t) + f_2(t)g_2(t))x_1 + \frac{\sigma_2(t)}{4}\right] \qquad \text{(B.3}b\text{)}$$

$$z_3(t) = 4\left[(f_3(t)h_3(t) + f_4(t)h_4(t))x_1 + (l_2(t)h_2(t) - l_1(t)h_1(t))x_4 + \frac{\sigma_3(t)}{4}\right] \qquad \text{(B.3}c\text{)}$$

$$z_4(t) = 4\left[(g_2(t)l_2(t) + l_1(t)g_1(t))x_2 - (l_2(t)h_2(t) - l_1(t)h_1(t))x_3 + \frac{\sigma_4(t)}{4}\right] \qquad \text{(B.3}d\text{)}$$

and

$$\nu_1(t) = \bar{\alpha}_1(t)f_1(t) + \mathrm{i}\bar{\alpha}_2(t)g_1(t) + \mathrm{i}\bar{\alpha}_3^*(t)h_1(t) - \bar{\alpha}_4^*(t)l_1(t) \qquad \text{(B.4}a\text{)}$$

$$\nu_3(t) = \bar{\alpha}_3(t)h_3(t) + \mathrm{i}\bar{\alpha}_4(t)l_3(t) + \mathrm{i}\bar{\alpha}_1^*(t)f_3(t) - \bar{\alpha}_2^*(t)g_3(t) \qquad \text{(B.4}b\text{)}$$

$$\begin{aligned}\sigma_1(t) = {} & f_2(t)(\nu_2^*(t) + \nu_2(t)) + \mathrm{i}f_1(t)(\nu_1^*(t) - \nu_1(t)) \\ & + f_3(t)(\nu_3^*(t) + \nu_3(t)) + \mathrm{i}f_4(t)(\nu_4^*(t) - \nu_4(t)) \qquad \text{(B.5}a\text{)}\end{aligned}$$

$$\begin{aligned}\sigma_3(t) = {} & h_1(t)(\nu_1^*(t) + \nu_1(t)) + \mathrm{i}h_2(t)(\nu_2^*(t) - \nu_2(t)) \\ & + \mathrm{i}h_3(t)(\nu_3^*(t) - \nu_3(t)) - h_4(t)(\nu_4^*(t) + \nu_4(t)) \qquad \text{(B.5}b\text{)}\end{aligned}$$

$$\beta_1^2(t) = \sum_{j=1}^{4}(f_j^2(t)\cos^2\bar{\theta} + l_j^2(t)\sin^2\bar{\theta}) - 2(f_2(t)l_2(t) + f_1(t)l_1(t))\sin(2\bar{\theta}) \qquad \text{(B.6}a\text{)}$$

$$\beta_2^2(t) = \sum_{j=1}^{4}(f_j^2(t)\sin^2\bar{\theta} + l_j^2(t)\cos^2\bar{\theta}) + 2(f_2(t)l_2(t) + f_1(t)l_1(t))\sin(2\bar{\theta}) \qquad \text{(B.6}b\text{)}$$

$$\beta_3^2(t) = \sum_{j=1}^{4}(g_j^2(t)\cos^2\bar{\phi} + h_j^2(t)\sin^2\bar{\phi}) + 2(g_4(t)h_4(t) - h_3(t)g_3(t))\sin(2\bar{\phi}) \qquad \text{(B.6}c\text{)}$$

$$\beta_4^2(t) = \sum_{j=1}^{4}(h_j^2(t)\cos^2\bar{\phi} + g_j^2(t)\sin^2\bar{\phi}) - 2(g_4(t)h_4(t) - h_3(t)g_3(t))\sin(2\bar{\phi}). \qquad \text{(B.6}d\text{)}$$

Furthermore,

$$\xi_1(t) = f_1(t)(\nu_1^*(t) + \nu_1(t)) - \mathrm{i} f_2(t)(\nu_2^*(t) - \nu_2(t)) + \mathrm{i} f_3(t)(\nu_3^*(t) - \nu_3(t)) - f_4(t)(\nu_4^*(t) + \nu_4(t)) \tag{B.7a}$$

$$\xi_3(t) = \mathrm{i} h_1(t)(\nu_1^*(t) - \nu_1(t)) - h_2(t)(\nu_2^*(t) + \nu_2(t)) + h_3(t)(\nu_3^*(t) + \nu_3(t)) + \mathrm{i} h_4(t)(\nu_4^*(t) - \nu_4(t)) \tag{B.7b}$$

where the following notations have been used:

$$\bar{\theta}(t) = \frac{1}{2}\tan^{-1}\left[\frac{4(f_2(t)l_2(t) + f_1(t)l_1(t))}{\sum_{j=1}^{4}(l_j^2(t) - f_j^2(t))}\right]$$
$$\bar{\phi}(t) = \frac{1}{2}\tan^{-1}\left[\frac{4(g_4(t)h_4(t) - h_3(t)g_3(t))}{\sum_{j=1}^{4}(g_j^2(t) - h_j^2(t))}\right] \tag{B.8}$$

taking into account that the other unmentioned quantities may be obtained by means of transformation (2.8).

References

[1] Li Kamwa P, Stitch J E, Mason N J, Roberts J S and Robson P N 1985 *Electron. Lett.* **21** 26
[2] Jin R, Chuang C L, Gibbs H H, Koch S W, Polky J N and Pubanz G A 1986 *Appl. Phys. Lett.* **49** 110
[3] Gusovkii D D, Dianov E M, Mairer A A, Neustreuev V B, Shklovskii E I and Scherbakov I A 1985 *Sov. J. Quantum Electron.* **15** 1523
[4] Townsend P D, Baker G L, Shelburne J L III and Etemad S 1989 *SPIE* **1147** 256
[5] Jensen S M 1982 *IEE J. Quantum Electron.* **18** 1580
Maier A A 1982 *Kvantovaya Elektron.* **9** 2296 (in Russian)
[6] Peřina J 1995 *J. Mod. Opt.* **42** 1517
[7] Peřina J and Bajer J 1995 *J. Mod. Opt.* **42** 2337
[8] Peřina J and Peřina J Jr 1995 *Quantum Semiclass. Opt.* **7** 849
[9] Peřina J and Peřina J Jr 1996 *J. Mod. Opt.* **43** 1951
[10] Peřina J and Peřina J Jr 1997 *Quantum Semiclass. Opt.* **9** 443
[11] Janszky J, Petak A, Sibilia C, Bertolotti M and Adam P 1995 *Quantum Semiclass. Opt.* **7** 145
[12] Karpierz M A, Kujawski A and Szczepański P 1995 *J. Mod. Opt.* **42** 1079
[13] Re A, Sibilia C, Fazio E and Bertolotti M 1995 *J. Mod. Opt.* **42** 82
[14] Assanto G, Palma Laureti A, Sibilia C and Bertolotti M 1994 *Opt. Commun.* **110** 599
[15] Janszky J, Sibilia C and Berolotti M, Adam P and Petak A 1995 *Quantum Semiclass. Opt.* **7** 509
[16] Berger P R, Bhattacharya P K and Gupta S 1991 *IEEE J. Quantum Electron.* **27** 788
[17] Dios F, Nogués X and Canal F 1992 *Opt. Quantum Electron.* **24** 1191
[18] Korolkova N and Peřina J 1996 *Opt. Commun.* **136** 135
[19] Chefles A and Barnett S M 1996 *J. Mod. Opt.* **43** 709
[20] Thylén L, Wright E M, Seaton G I and Moloney J V 1986 *Opt. Lett.* **11** 739
[21] Yasumoto K, Maeda H and Maekawa N 1996 *J. Lightwave Technol.* **14** 628
[22] Peřina J and Peřina J Jr 1997 *Quantum Semiclass. Opt.* **51** 443
[23] Jaynes E T and Cumming F W 1963 *Proc. IEEE* **51** 89
[24] Peřina J and Křepelka J 1991 *J. Mod. Opt.* **38** 2137
[25] Assanto G, Stegeman G, Sneik-Bahae M and Van Stryland E 1993 *Appl. Phys. Lett.* **62** 1323
[26] Yariv A and Yeh P 1984 *Optical Waves in Crystals* (New York: Wiley) p 389
[27] Peřina J, Peřinová V and Kodousek J 1984 *Opt. Commun.* **49** 210
[28] Kielich S, Tanaś R and Zawodny R 1987 *J. Opt. Soc. Am.* B **4** 1627
[29] Peřina J, Peřinová V, Sibilia C and Bertolotti M 1984 *Opt. Commun.* **49** 285
[30] Razmi M S K and Eberly J H 1990 *Opt. Commun.* **76** 265
[31] Kumar A and Gupta P S 1995 *Quantum Semiclass. Opt.* **7** 835
[32] Kumar A and Gupta P S 1996 *Quantum Semiclass. Opt.* **8** 1053
[33] Loudon R and Knight P L 1987 *J. Mod. Opt.* **34** 709
[34] Caves C M and Schumaker B L 1985 *Phys. Rev.* A **31** 3068
Caves C M and Schumaker B L 1985 *Phys. Rev.* A **31** 3093

[35] Collett M J and Gardiner C W 1985 *Phys. Rev.* A **30** 1386
Collett M J and Loudon R 1987 *J. Opt. Soc. Am.* B **4** 1525
[36] Mollow B R and Glauber R J 1967 *Phys. Rev.* **160** 1076
[37] Singh S 1983 *Opt. Commun.* **44** 254
[38] Zou X T and Mandel L 1990 *Phys. Rev.* A **41** 475
[39] Miranowicz A, Bajer J, Ekert A and Leoński W 1997 *Acta Phys. Slovaca* **47** 319
Miranowicz A, Bajer J, Matsueda H, Wahiddin M R B and Tanaś R 1999 *J. Opt. Soc. Am.* B submitted
Miranowicz A, Bajer J, Matsueda H, Wahiddin M R B and Tanaś R 1999 *J. Opt. Soc. Am.* A submitted
[40] Cahill K E and Glauber R J 1969 *Phys. Rev.* **177** 1857
Cahill K E and Glauber R J 1969 *Phys. Rev.* **177** 1882
[41] Hong C K and Mandel L 1985 *Phys. Rev.* A **32** 974
[42] Agarwal G S 1986 *Phys. Rev.* A **34** 4055
[43] Agarwal G S 1987 *J. Mod. Opt.* **34** 909
[44] Louisell W H 1973 *Quantum Statistical Properties of Radiation* (New York: Wiley) p 175
[45] Lai W K, Bužek V and Knight P L 1991 *Phys. Rev.* A **43** 6323
[46] De Oliveira F A M, Kim M S and Knight P L 1990 *Phys. Rev.* A **41** 2645
[47] Janszky J, Sibilia C and Bertolotti M 1991 *J. Mod. Opt.* **38** 2467